

**CHARACTERIZATION OF THE PURDUE EXPERIMENTAL TURBINE
AEROTHERMAL LAB RIG USING HOT WIRES**

by

Swapnil Sushil Ingale

A Thesis

Submitted to the Faculty of Purdue University

In Partial Fulfillment of the Requirements for the degree of

Master of Science in Mechanical Engineering



School of Mechanical Engineering

West Lafayette, Indiana

December 2018

**THE PURDUE UNIVERSITY GRADUATE SCHOOL
STATEMENT OF COMMITTEE APPROVAL**

Dr. Guillermo Paniagua, Chair

Department of Mechanical Engineering

Dr. Paul E. Sojka

Department of Mechanical Engineering

Dr. Patricia Davies

Department of Mechanical Engineering

Approved by:

Dr. Jay P Gore

Head of the Graduate Program

*Dedicated to
My Family and Friends*

ACKNOWLEDGMENTS

The author would like to thank Dr. Guillermo Paniagua, Dr. Patricia Davies and Dr. Paul E. Sojka for their guidance. The author would like to thank Jorge Savedra for the help and support given during the complete thesis work. The author would like to thank Lakshya Bhatnagar for the help during the experiment. The author would like to thank all the Petal team for their continued support and motivation. The author would like to thank his parents for their support.

TABLE OF CONTENTS

LIST OF TABLES	vii
LIST OF FIGURES	viii
NOMENCLATURE	x
ABSTRACT.....	xii
1. INTRODUCTION.....	1
1.1 Objectives	1
1.2 Methodology.....	1
1.2.1 Development of Hot Wire Anemometry System.....	1
1.2.2 Develop the Needed Hardware for the Test Section	2
1.2.3 Characterization of the Flow Velocity.....	2
1.3 Structure.....	2
2. HOT WIRE ANEMOMETRY AND EXPERIMENTAL SETUP.....	4
2.1 Review of hot wire anemometry and experimental setup.....	4
2.1.1 Hot Wire Anemometry	4
2.1.2 Experimental Setup.....	8
2.2 Hot wire calibration procedure and post process	13
2.2.1 Review of Hot Wire Calibration.....	13
2.2.2 Post Process	16
3. MODERN MANUFACTURING TECHNIQUES FOR THE DEVELOPMENT OF THE LAB	20
3.1 Abrasive Cutting Operation	20
3.2 Cold Machining Operations.....	22
3.2.1 Milling	23
3.2.2 Turning	24
3.3 Manufactured Equipment.....	26
4. EXPERIMENTAL RESULTS	29
4.1 Selection of Time Window:.....	29
4.2 Hot Wire Calibration Results.....	31

4.2.1	Pressure Data	31
4.2.2	Temperature Data	33
4.2.3	Hot Wire Voltage Data	34
4.2.4	Hot Wire Calibration Result	35
4.3	Hot Wire Post Process Results.....	36
4.4	Uncertainty Analysis.....	40
5.	CONCLUSIONS	43
	APPENDIX.....	44
	REFERENCES	45

LIST OF TABLES

Table 4.1 Calibration data of the pressure sensors with standard deviation of the estimated mean in magnitude of 10^{-1} Pa.	31
Table 4.2 Calibration data of the Temperature with standard deviation of the estimated mean in magnitude of 10^{-3} K.	34
Table 4.3 Calibration data of the Hot Wire sensor with standard deviation of the estimated mean in magnitude of 10^{-4} V.	35
Table 4.4 Calibration data of velocity.....	35
Table 4.5 Turbulent property.	37
Table 4.6 Integral length scale ratio data.	39
Table 4.7 Uncertainty calculation for velocity.	41
Table 4.8 Uncertainty calculation for Turbulence intensity.	42
Table 4.9 Uncertainty calculation for Integral length scale.	42
Table 4.10 Uncertainty calculation for Dissipative length scale.	42

LIST OF FIGURES

Figure 2.1 Calibration results using King’s Law (Figure reproduced with permission of publisher) [1].....	5
Figure 2.2 Calibration results including Collis and Williams correction (Figure reproduced with permission of publisher) [1].....	6
Figure 2.3 Constant Temperature Anemometer (CTA) circuit [8].	7
Figure 2.4 Design of the test cell (Figure reproduced with permission of publisher) [9].....	8
Figure 2.5 a) Linear test section b) dimension of linear test section c) cross-sectional view of linear test section and d) operating limits (Figure reproduced with permission of publisher) [9].....	9
Figure 2.6 Overall view of the experimental setup a) test cell b) linear wind tunnel test section and c) CTA module setup.	10
Figure 2.7 Hot wire schematics (Figure reproduced by permission of manufacturer) [24].	10
Figure 2.8 Sensor assembly over a flat plate.	11
Figure 2.9 Oscilloscope used for a) checking the pulse response and b) setting up the DC offset and gain.	12
Figure 2.10 Pulse response [10].....	13
Figure 2.11 Overview of the Hot Wire Calibration.	14
Figure 2.12 Post process methodology.	17
Figure 3.1 Waterjet nozzle operation [11].	21
Figure 3.2 Waterjet machine at BIDC.	22
Figure 3.3 3-Axis CNC milling machine.....	23
Figure 3.4 5-Axis CNC milling machine.....	24
Figure 3.5 CNC lathe machine.....	25
Figure 3.6 Instrumentation equipment: a) insert1 b) insert2 c) support and d) assembly.	27
Figure 3.7 Graphoil gasket a) manufacturing of the gasket and b) manufactured gasket.	28
Figure 4.1 Time window selection for a) total pressure and b) total temperature.	30
Figure 4.2 Static pressure in a stable region for three different velocities.	32
Figure 4.3 Total pressure in a stable region for three different velocities.	32
Figure 4.4 Total temperature data in a stable region for three different velocities.....	33

Figure 4.5 Voltage of hot wire in a stable region for three different velocities.....	34
Figure 4.6 Curve fitting plot.	36
Figure 4.7 Velocity plot in a stable region for three different velocities.....	37
Figure 4.8 Turbulence properties plotted against velocity a) turbulence intensity (%) b) integral length scale and c) dissipative length scale.....	38
Figure 4.9 a) Honeycomb structure and b) ILR vs velocity plot.	39

NOMENCLATURE

List of Symbols

A	Calibration constant
B	Calibration constant
C	Random dependent variable
E	Hot wire voltage
E^*	Equivalent voltage
E'	Voltage fluctuation
M	Mach number
n	Calibration constant
np	Number of data points
N	Nusselt number
P_0	Total pressure
P_s	Static pressure
R	Gas constant
R_0	Initial hot wire resistance
Re	Reynold's number
T_{film}	Film temperature
T_m	Film temperature
T_∞	Free stream temperature
T_0	Total Pressure
T_{gas}	Temperature of gas
U	Flow velocity
V	Velocity of flow
V^*	Equivalent velocity
X	Random independent variable
Y	Measured value
Z	Predicted value
γ	Specific heat ratio
μ	Dynamic viscosity

ρ	Density of the film
α_0	Coefficient of resistivity

List of Abbreviations

CAD	Computer Aided Design
CAM	Computer Aided Manufacturing
CCA	Constant Current Anemometer
CNC	Computer Numerical Control
CTA	Constant Temperature Anemometer
DC	Direct Current
DLS	Dissipative length scale
HWA	Hot Wire Anemometry
ILS	Integral length scale
LDS	Laser Doppler Anemometers
Tu	Turbulence intensity

ABSTRACT

Author: Ingale, Swapnil, S. MSME

Institution: Purdue University

Degree Received: December 2018

Title: Characterization of the Purdue Experimental Turbine Aerothermal Lab Rig using Hot Wires

Major Professor: Guillermo Paniagua

The objective of this thesis is to apply high frequency flow measurement technique known as hot wire anemometry to characterize the velocity, turbulence intensity and turbulent length scales in the Purdue Experimental Turbine Aerothermal Lab Rig. Hot wire anemometry has been widely used to characterize velocities and turbulence levels in different environments and using different calibration and post-processing methodologies. In this work, a precise calibration and post-processing method was developed and successfully applied to the state-of-the-art trisonic Purdue Experimental Turbine Aerothermal Lab wind tunnel. The different experimental setups where the turbulence levels were analyzed were fabricated using modern manufacturing techniques such as 3D printing or water cutting. These techniques increase the complexity of the designs to be tested in wind tunnels. Calibration process was then successfully tested in the Purdue Experimental Turbine Aerothermal Lab Rig. Finally, accuracy and sensitivity analysis of the calibration are performed to verify the performance and reliability of the process.

1. INTRODUCTION

1.1 Objectives

The purpose of this work is to characterize the Purdue Experimental Turbine Aerothermal Lab rig. To achieve this goal hot wire anemometry measurements were used. The sensor used is generally known as a Hot wire. The probe used in this work has a frequency response up to 250 kHz and a maximum operating fluid temperature of 300⁰C. The sensor is very sensitive to the flow changes and hence was chosen to find out the turbulent properties of the flow. To measure the accuracy of the sensor the precise uncertainty measurements are done for the experiments.

Hence the objective of this work are listed as following:

1. Development Hot Wire Anemometry system
2. Develop the needed hardware for the test section
3. Characterization of the flow velocity

1.2 Methodology

To achieve the objective of this work, an amalgamation of theoretical and experimental methods has been used. To select the proper technique extensive literature review is done. Through it, we have developed the hot wire anemometry technique as our principle method. The developed hot wire anemometry technique was tested in the linear wind tunnel with flat plate. Afterword's the hot wire technique was used in multiple tests to analyze the spatial and temporal uniformity of the Purdue Experimental Turbine Aerothermal Lab rig.

1.2.1 Development of Hot Wire Anemometry System

After selecting the hot wire anemometry as our principle method to get the characterization, a suitable data acquisition procedure is needed for the successful employment of the sensor. Development of this data acquisition procedure was fundamentally based on using the already existing sensors in experimental lab, which includes temperature sensors, pressure sensors. For the operation of the hot-wire sensor, total pressure sensors, static pressure sensors, total temperature sensors were used to develop the technique.

Hot wire calibration is done before every experiment. In this process we use the available pressure and temperature sensors to calculate the flow velocity and match it with the Hot wire sensor using proper calibration process. The calibration process was done in the linear wind tunnel. For the calibration process, we will be using the CTA module, total pressure sensors, static pressure sensors, total temperature sensors. During the calibration we will choose stable data points to find out the calibration. During the calibration process minor adjustments are also made to make sure the hot wire response is within the acceptable range of the data acquisition system.

1.2.2 Develop the Needed Hardware for the Test Section

In research, there is often a need for custom instrumentation and parts. Such components are generally contracted out to companies for manufacture. This process consumes significant amount of time and research funding. To resolve this problem, we came up with the inhouse manufacturing as our solution. Inhouse manufacturing provides us with the benefit of low cost of operation and less time in manufacturing. For this, various modern manufacturing techniques were investigated to better understand the manufacturing process. Using these techniques, we built needed hardware for the experiment.

1.2.3 Characterization of the Flow Velocity

Once the hot wire is calibrated, it can be used in various experimental campaigns. To use in any experimental campaign, we need to install hot wire, along with its CTA module, pressure sensors and temperature sensors. Once the data is collected through data acquisition system, we post process the data to get various turbulent properties. We calculate velocity of the flow, turbulence intensity, length scales and uncertainty to achieve the goals of the experimental campaign.

1.3 Structure

This dissertation is divided into four chapters. Chapter 1 is an overview on the objectives and methodology of this work.

In Chapter 2 the hot wire anemometry and its advantages over a competitive technique, Laser Doppler Anemometer is described. In this chapter previous works on the topic of hot wire anemometry are summarized. This chapter further explains the experimental equipment and setup

that has been used for this work. This chapter also illustrates the hot wire calibration and hot wire post process.

In Chapter 3 multiple inhouse modern manufacturing techniques that were used in the development of the lab. It also gives a perspective on how these methods are able to help in the progress of the research and why they are so important to understand.

In Chapter 4 the experimental results that have been carried out with the hot wire. This chapter gives details about the pressure data, temperature data, hot wire data. It also shows the hot wire calibration results and hot wire post process results that will help in characterizing the Purdue Experimental Turbine Aerothermal Lab rig.

Chapter 5 concludes with the findings of this work.

2. HOT WIRE ANEMOMETRY AND EXPERIMENTAL SETUP

2.1 Review of hot wire anemometry and experimental setup

2.1.1 Hot Wire Anemometry

Hot Wire Anemometry can be defined as: The measurement of fluid flow using the variations in heat transfer from an electrically heated element exposed to the flow [5]. Hot Wire Anemometry (HWA) is a measurement technique used to characterize the flow.

According to H. H. Bruun [4] Hot wire anemometry has following advantages over its competitor techniques, Laser Doppler Anemometers (LDA):

- i. Cost: HWA systems are relatively cheaper
- ii. Frequency response: HWA have higher frequency response than LDA
- iii. Size: Hot wire sensors are relatively in smaller size
- iv. Velocity measurement: Although both systems have very wide range of velocity measurement, HWA has advantage in finding out 1-D, 2-D, 3-D flow characteristics using different types of hot wires
- v. Two phase flow: HWA system performance exceptionally well compared to LDA system in two phase flows
- vi. Operation: HWA system is relatively easy operate, calibrate and analyze
- vii. Spatial characterization: Using multiple hot wire sensors we can easily analyze the spatial characteristics of the flow

In the review by L. M. Fingerson [5] mention that HWA techniques dates back 1817. Since then this technique came far, lot of new work has been added and it evolved to the current state. The current work in HWA started with King [6], when he published his work on Convective heat transfer over small cylinders. In his work he proposed the following power law, Equation (2.1)

$$E^2 = A + BU^n \quad (2.1)$$

Researchers after him further improved on his work, and one of the noticeable contributions was done by Collis and Williams [7] who used the temperature loading to further improve the relation. The Nusselt co-relation proposed by Collis and Williams [7] is presented in Equation (2.2), where N is Nusselt number, Re is Reynold's number, T_m is film temperature, T_∞ is free stream temperature, A and B are constants

$$N \left(\frac{T_m}{T_\infty} \right)^{-0.17} = A + B Re^n \quad (2.2)$$

In this expression values of A , B and n depends upon the Reynold's number for which vortex street exists. Collis and Williams have validated their findings at low Reynold's number with the Ossen method.

This is method was implemented by T. Yasa et al. [1] who included the Collis and Williams correlation to the calibration of the hot-wire. This helped in removing the temperature variation of the hot wire calibration as shown in Figure 2.1. Results of temperature correction are shown in Figure 2.2. The modified King's proposed equation used by Collis and Williams is shown in Equation 2.3.

$$\frac{E^2}{T_{wire} - T_{gas}} \left(\frac{T_{film}}{T_{gas}} \right)^{-0.17} = A + B \left(\frac{\rho_{film} \cdot u}{\mu_{film}} \right)^n \quad (2.3)$$

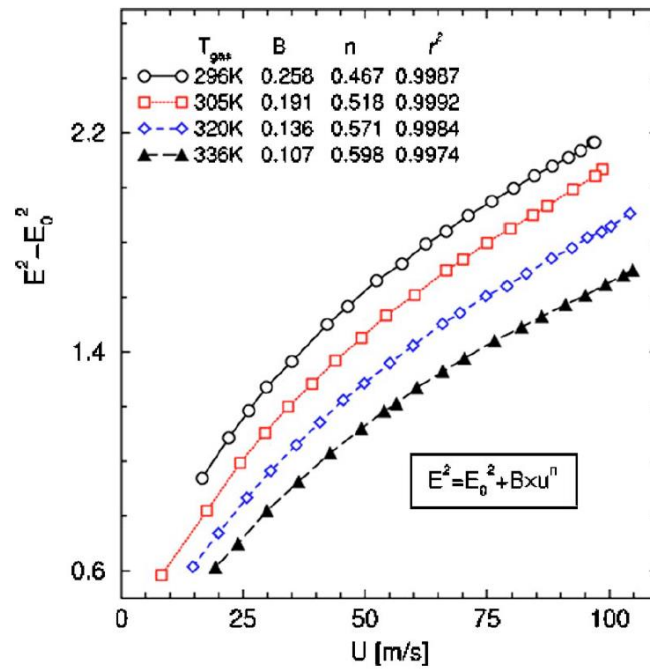


Figure 2.1 Calibration results using King's Law (Figure reproduced with permission of publisher) [1].

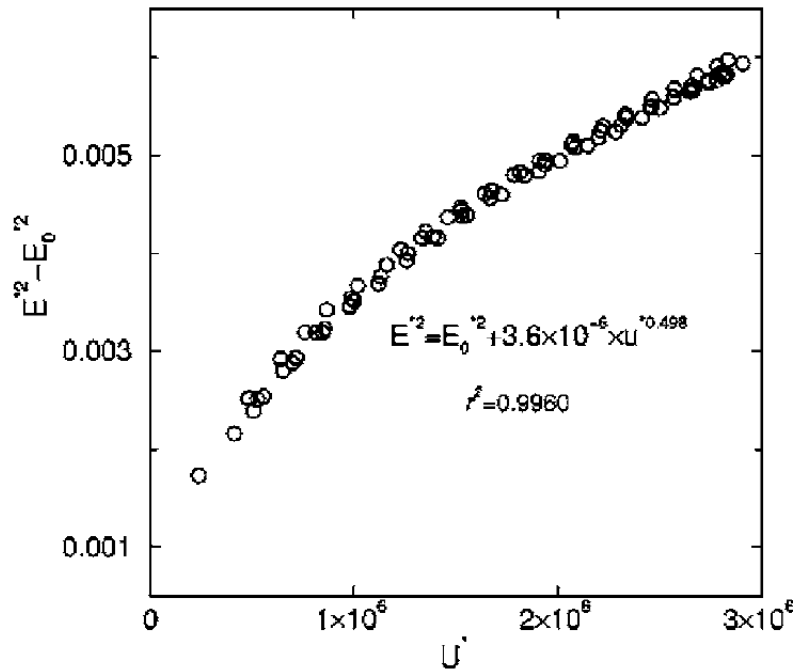


Figure 2.2 Calibration results including Collis and Williams correction (Figure reproduced with permission of publisher) [1].

In this work we are going to use the work of T. Yasa *et al.* [1] as our base to further develop the calibration and post process strategy.

This technique uses hot wires with conjunction with different types of anemometers. The frequently used anemometers are constant temperature anemometer (CTA) and constant current anemometer (CCA). For this work we have selected to work with constant temperature anemometer. In Hot Wire Anemometry measurement techniques, a thin hot wire is heated and exposed to the flows in interest. Operation of hot wire will be dependent on the type of anemometer. In CTA the temperature of the hot wire is kept constant while in CCA the current in the hot wire is kept constant. Nowadays CTA modules are used more than CCA modules because of its ease of application and high signal to noise ratio.

According to H. H. Bruun [6], researchers started to realize the advantages of the constant temperature anemometer in 1940s but the reliable devices were not available until 1960s. Figure 2.3 shows the circuit used in the Constant Temperature Anemometer.

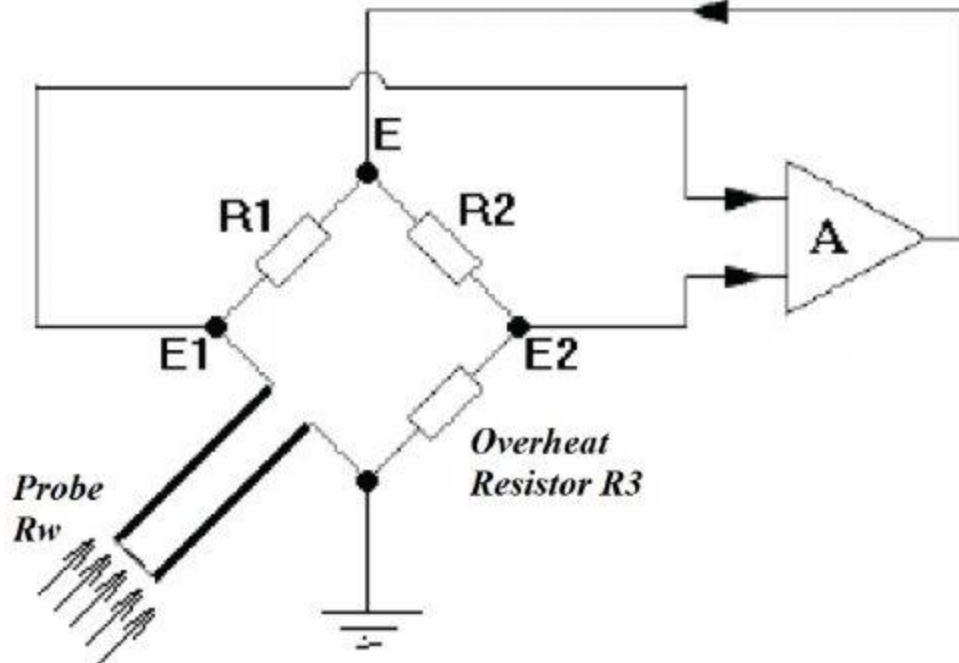


Figure 2.3 Constant Temperature Anemometer (CTA) circuit [8].

As shown in the above Figure 2.3, the base of the electrical circuit is made up of well-known Wheatstone bridge. As the flow condition changes, the voltage difference ($E1-E2$) changes with it. This change indicates the change in the resistance of the probe wire. The difference of this voltages is sent to the amplifier A which in turn generates a feedback current, which is fed to the Wheatstone bridge. When you feed this current to the bridge it restores the probe wire's resistance back to its original value. Keeping the resistance of the wire constant also keeps the temperature of hot wire at constant.

Modern commercially available constant temperatures anemometer contains many options:

- i. Filter with different bands
- ii. Fixed or variable gain
- iii. DC offset
- iv. Temperature compensation modules
- v. Inbuilt low pass filter
- vi. Multiple frequency response setup

This flexibility in the device configuration allows it to be used in different applications and flow conditions. It allowed users to condition their systems to their need.

2.1.2 Experimental Setup

For this work all the experiments and calibration were done in the the Purdue experimental turbine aerothermal lab rig situated at Zucrow laboratories which is a part of Purdue University. Design of the lab is shown in Figure 2.4.

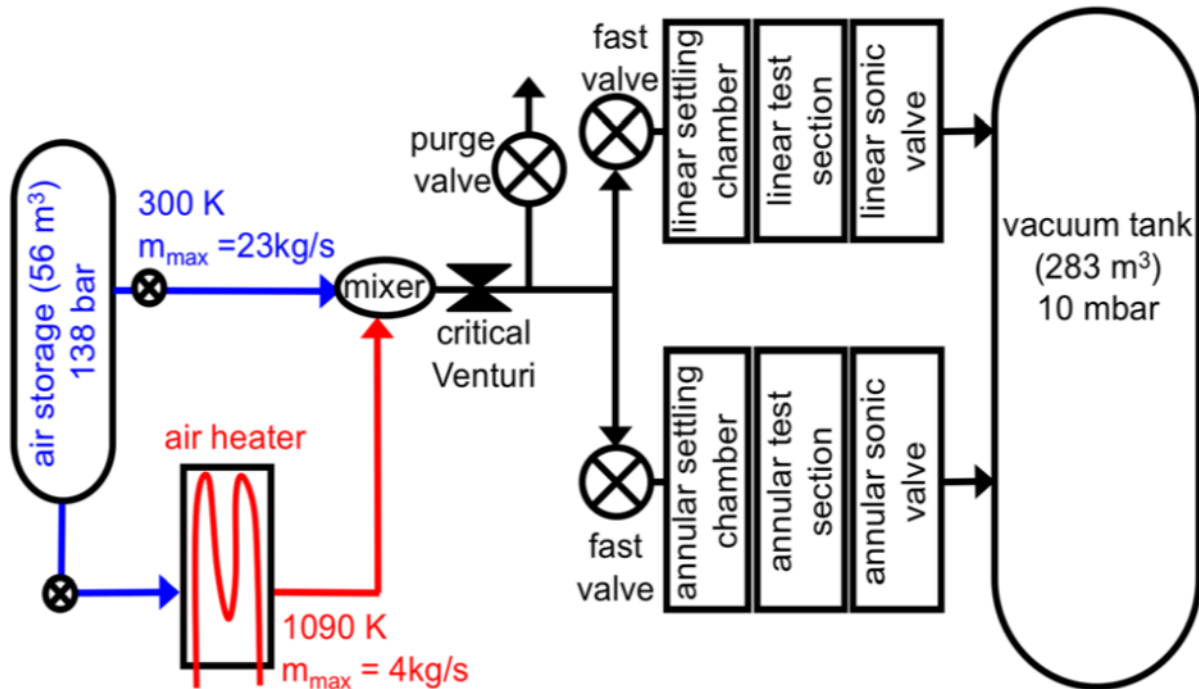


Figure 2.4 Design of the test cell (Figure reproduced with permission of publisher) [9].

For this work we have used the linear test section. This facility is equipped with a tank that stores air at ambient temperature and it can be pressurized up to 150 bar. It also equipped with the air heater which provides heated air which then passes through the mixer and can provide air in a pressure range of 0.5 bar to 6 bar and temperature range of 270K to 700K in the test section. This helps in attain a very large range of Reynolds number and velocities in the test section.

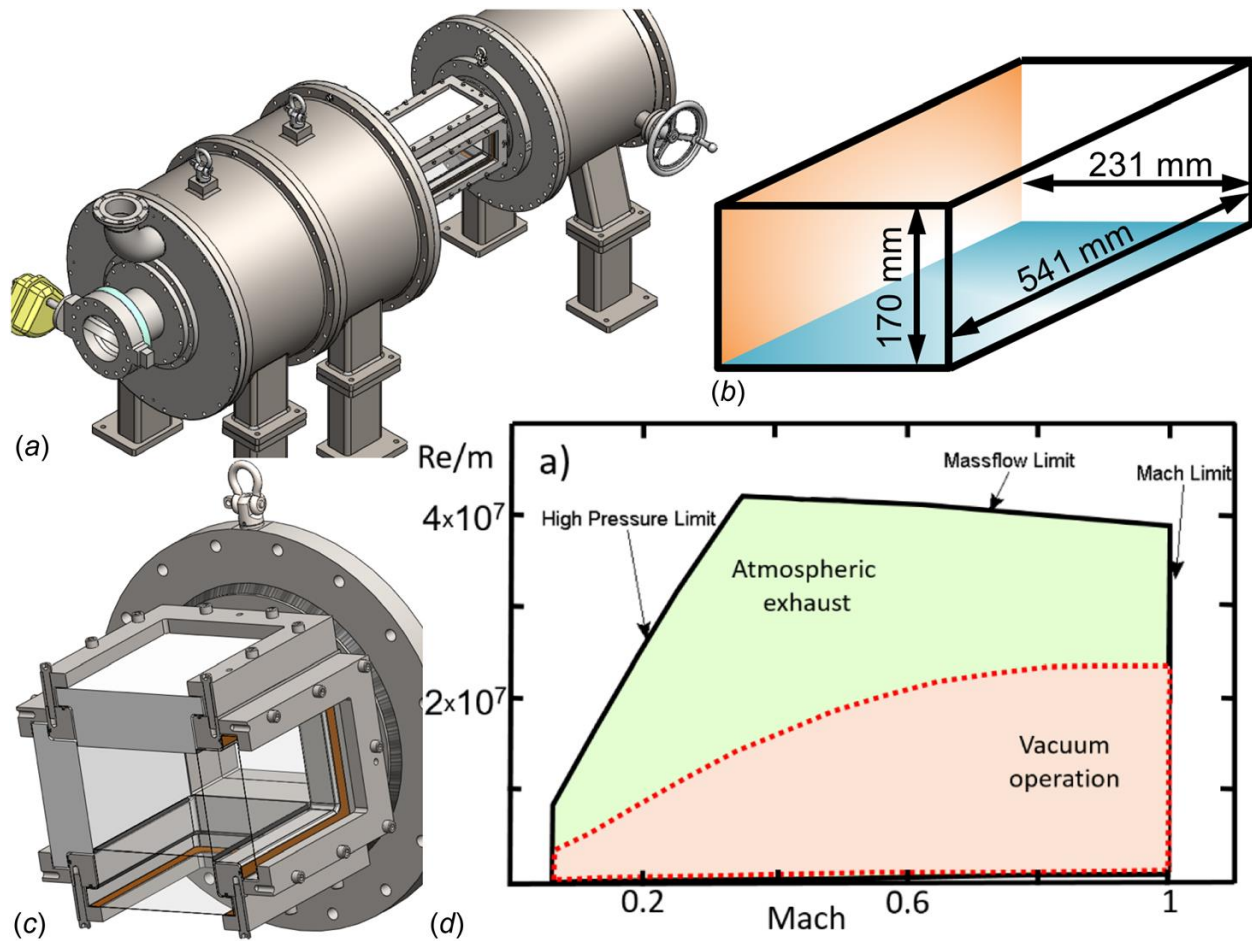


Figure 2.5 a) Linear test section b) dimension of linear test section c) cross-sectional view of linear test section and d) operating limits (Figure reproduced with permission of publisher) [9].

In Figure 2.5 the linear test section is shown. Each separated part is hold together by bolts and they are sealed using O-rings are gaskets to make sure there is no leakage in the test section.

In the Figure 2.6 the overall assembly of the test section is shown.

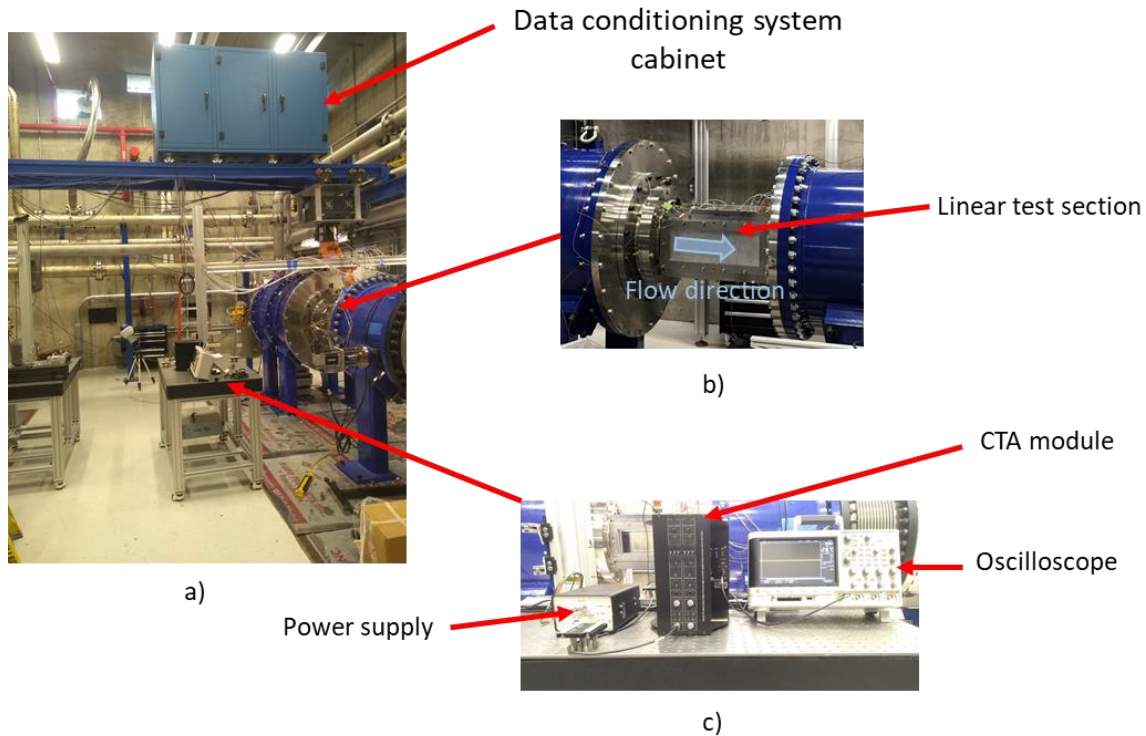


Figure 2.6 Overall view of the experimental setup a) test cell b) linear wind tunnel test section and c) CTA module setup.

Figure 2.6 shows the overall view of the experimental setup. The experiment was carried out in the linear wind tunnel as shown in the Figure 2.6 b). To start the experiment, we kept the CTA module, oscilloscope and main DC power supply on the optical table as shown in Figure 2.6 c). A cable of 5m is connecting the CTA module to the Hot-wire probe holder. A schematic of the hot wire probe used in the experiments is shown in the Figure 2.7.

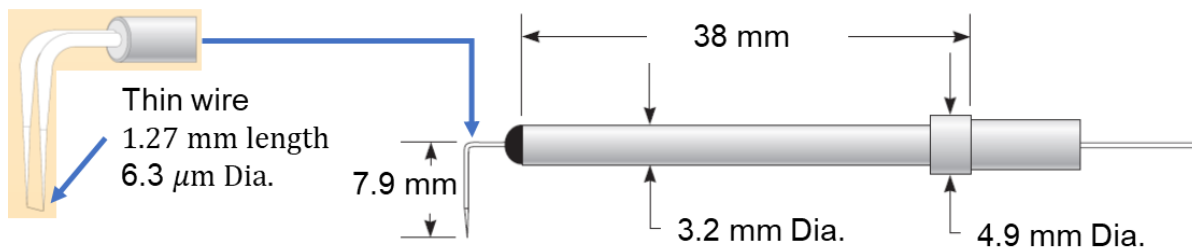


Figure 2.7 Hot wire schematics (Figure reproduced by permission of manufacturer) [24].



Figure 2.8 Sensor assembly over a flat plate.

The hot wire probe is held perpendicular to the flow direction inside the linear test section as shown in the Figure 2.8. All the different sensors including total pressure, static pressure, total temperature sensors are attached along with hot wire sensor as shown in Figure 2.8.

We have calibrated the hot wire in the flat plate test article as shown in Figure 2.8. We chose the flat plate to calibrate because of the linearity we can achieve in that test section. The more stable the data, the better will be the accuracy of the calibration process.

The pre-operation procedure for the hot wire:

- i. Measure the Hot wire resistance
- ii. Apply over heat ratio (OHR) of 1.3
- iii. Put the DC offset and gain for the hot wire as shown in Figure 2.9 b)
- iv. Check the pulse response as shown in Figure 2.9 a)
- v. Select the frequency response

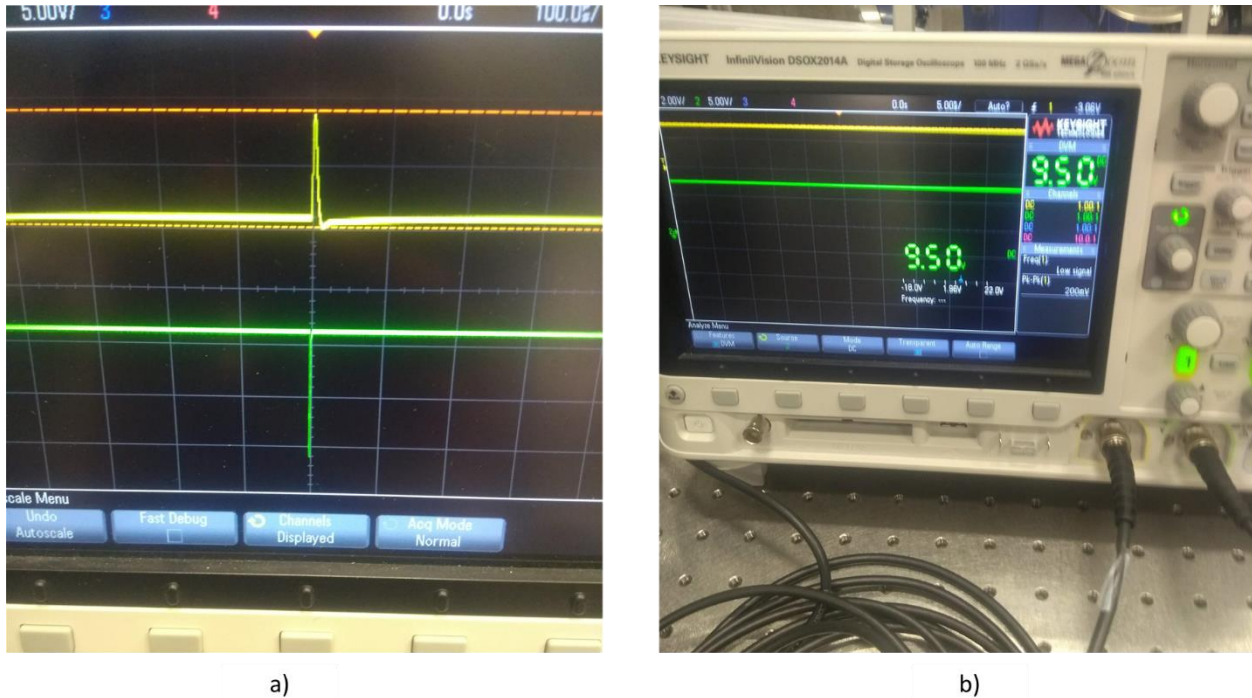


Figure 2.9 Oscilloscope used for a) checking the pulse response and b) setting up the DC offset and gain.

Value for the DC offset is decided by the data acquisition system limit. The range of the voltage it can read is from -10V to 10V. The hot wire voltage decreases with increase in velocity therefore the DC offset is set between 9.5V to 9.75V. To set that we need to make sure that hot wire is experiencing the zero velocity during pre-operation procedure. Gain of the hot wire is decided based on the operational limits. Once the gains are set, they can be tested to verify whether they are in the same limits or not. If not then, we can adjust them to match the requirements. There is another important step to do and that is checking out the pulse response. This step is necessary to make sure when the hot wire is in the operational mode it is not subject to oscillations, because oscillations destroy the CTA module. The oscillations are adjusted using the damping and tuning coil situated on the CTA module. Figure 2.10 shows what is desired and what is not desirable. Figure 2.9 a) shows the actual response tested during the procedure.

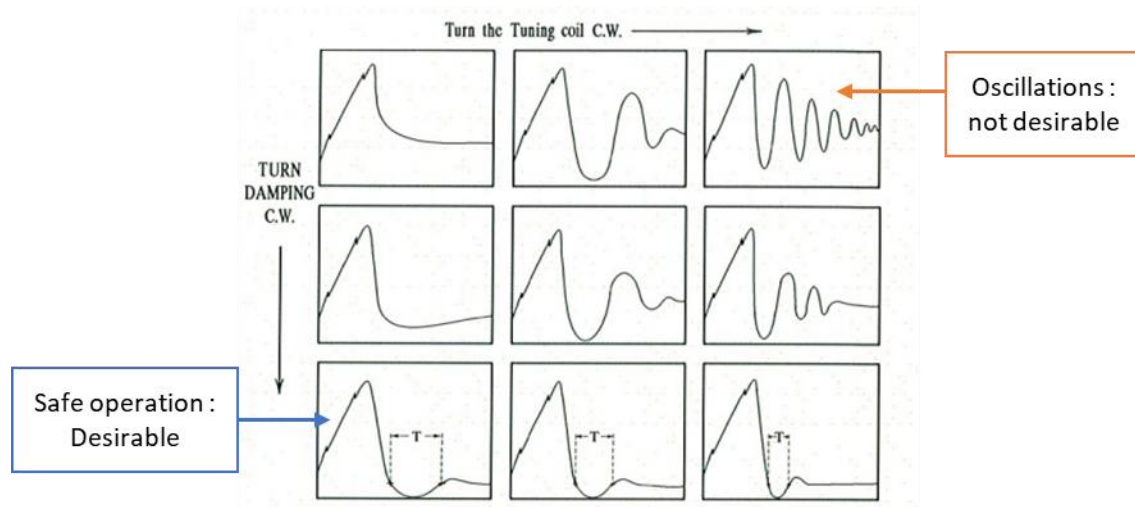


Figure 2.10 Pulse response [10].

Once the pulse response is checked we select the cut off frequencies, filter bands for our operation. Now we check the data connection for any irregular signals. Once that is checked the hot wire is ready for calibration and experiments.

2.2 Hot wire calibration procedure and post process

2.2.1 Review of Hot Wire Calibration

Here the calibration process of the hot wire is discussed. During the calibration experiment we use multiple sensor to measure the flow data. The sensors that are used for calibration are total pressure sensor, static pressure sensor, total temperature sensor, hot wire sensor and constant temperature anemometer (CTA) module. The process of the calibration is represented in the Figure 2.11.

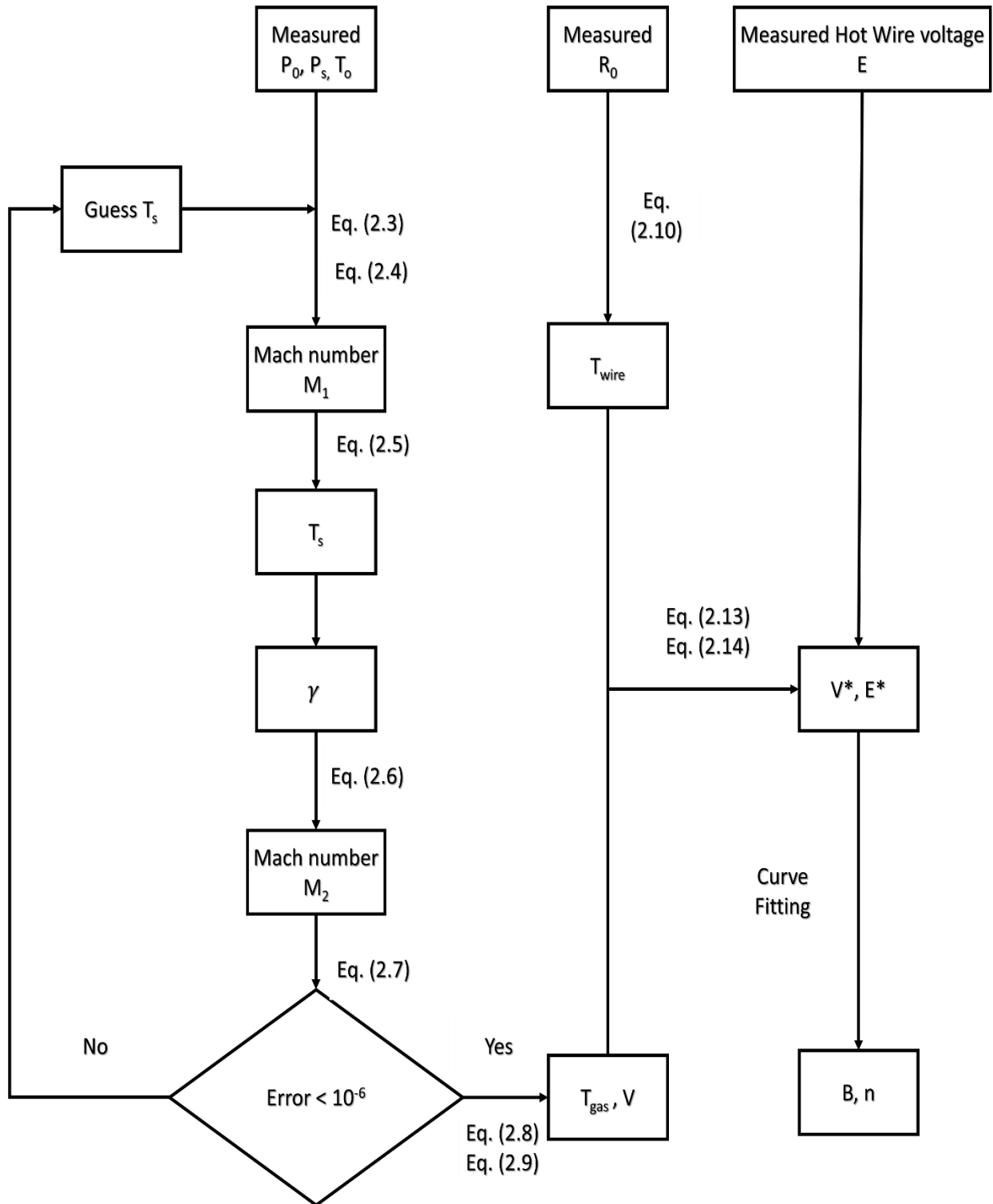


Figure 2.11 Overview of the Hot Wire Calibration.

As shown in the Figure 2.13 we can see that there are total five quantities we are measuring total pressure (P_0), static pressure (P_s), total temperature (T_0), initial hot wire resistance (R_0), hot wire voltage (E). To calculate the velocity and temperature of the flow we are going to use iterative process to minimize the error. The iterative process starts with initial assumption of T_s , in our case we are stating with

$$T_s = T_0 \quad (2.3)$$

Now we calculate the ratio of specific heat $\gamma(T_s)$ which is static temperature dependent property. Using the compressible flow properties, the Mach number (M_1) is calculated by using in Equation (2.4).

$$M_1 = \sqrt{\left(\frac{2}{\gamma - 1}\right) \left(\frac{P_s}{P_0}\right)^{\left(\frac{1-\gamma}{\gamma}-1\right)}} \quad (2.4)$$

The static temperature is re-estimated using the Equation (2.5).

$$T_s = \frac{T_0}{\left(1 + M_1^2 \left(\frac{\gamma - 1}{2}\right)\right)} \quad (2.5)$$

The value of the specific ratio (γ) with new static temperature (T_s) is re-estimated. Mach number (M_2) is calculated using Equation (2.6).

$$M_2 = \sqrt{\left(\frac{2}{\gamma - 1}\right) \left(\frac{P_s}{P_0}\right)^{\left(\frac{1-\gamma}{\gamma}-1\right)}} \quad (2.6)$$

Now we define an Error as shown in Equation (2.7). We iterate the above process until we get an error less than 10^{-6} .

$$Error = \left| \frac{M_2 - M_1}{M_1} \right| \quad (2.7)$$

Once the iteration ends, we get velocity of the flow (V) and temperature of gas (T_{gas}) using Equation (2.8) and Equation (2.9).

$$T_{gas} = T_s \quad (2.8)$$

$$V = M \sqrt{\gamma R T_{gas}} \quad (2.9)$$

Initial hot wire resistance (R_0) is calculated using the inbuilt voltmeter inside CTA module with least count of 0.01 V. Temperature coefficient of resistivity ($\alpha_0=0.0009\text{K}^{-1}$) was provided by the

manufacturer with uncertainty of 0.00005 K^{-1} . With the help of known temperature coefficient of resistivity and Over Heat Ratio (OHR), we can calculate the hot wire temperature (T_{wire}) using the Equation (2.10). Film properties are evaluated such as film temperature (T_{film}) and density of the film (ρ) using Equation (2.11) and Equation (2.12).

$$T_{wire} = T_0 + \frac{(OHR - 1)}{\alpha_0} \quad (2.10)$$

$$T_{film} = \frac{T_{wire} + T_{gas}}{2} \quad (2.11)$$

$$\rho = \frac{P_s}{(R \cdot T_{film})} \quad (2.12)$$

Now we calculate the equivalent velocity (V^*) and equivalent voltage (E^*) using Equation (2.13) and Equation (2.14) [1]. We also need to keep in mind that our equivalent voltage at velocity is zero if not we can shift the whole plot in a way it will give us zero equivalent voltage at zero velocity. This helps in reducing unknown constants, making the calibration more stable.

$$V^* = V \cdot \left(\frac{\rho}{\mu}\right) \quad (2.13)$$

$$E^* = E \cdot \sqrt{\frac{OHR \cdot R_0}{(T_{wire} - T_{gas})} \cdot \left(\frac{T_{film}}{T_{gas}}\right)^{-0.17}} \quad (2.14)$$

Once we get the equivalent voltage (E^*) and equivalent velocity (V^*), we will fit the data points around the Equation (2.15).

$$E^{*2} = B \cdot (V^*)^n \quad (2.15)$$

This helps in obtaining the unknown constants 'B' and 'n'. With this our calibration of the hot wire ends.

2.2.2 Post Process

Once the hot wire is calibrated it can be used in various experiments to characterize the flow. For a typical application hot wires are used to find the velocity and turbulence intensity of the flow. In this work hot wire is going to be used to find following properties of the flow in the inlet of the linear wind tunnel shown Figure 2.6 b) and Figure 2.8:

- i. velocity
- ii. turbulence intensity

iii. turbulence length scale

The process to find out these quantities is represented in Figure 2.12. This process is referenced from the post process methodology proposed by T. Yasa and G. Paniagua [1].

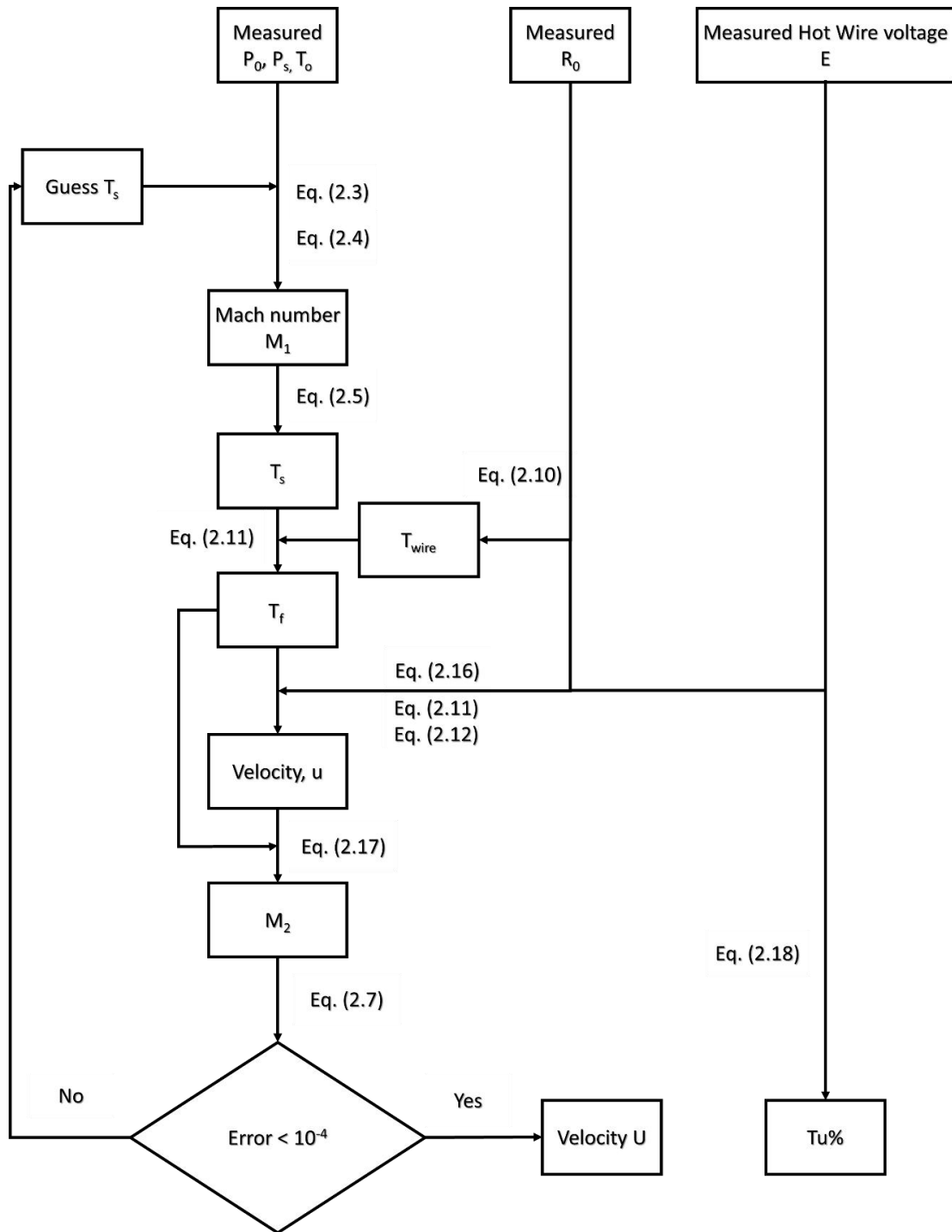


Figure 2.12 Post process methodology.

As shown in the Figure 2.12 we can see that there are total five quantities we are measuring total pressure (P_0), static pressure (P_s), total temperature (T_0), initial hot wire resistance (R_0), hot wire voltage (E). To calculate the velocity and temperature of the flow we are going to use iterative process to minimize the error. The iterative process starts with initial assumption of T_s , in our case we are stating with Equation (2.3).

Now we calculate the ratio of specific heat $\gamma(T_s)$ which is static temperature dependent property. Using the compressible flow properties, we are going to calculate Mach number (M_1) as shown in Equation (2.4).

Now we recalculate the static temperature using the Equation (2.5).

Using the CTA module, we to measure initial hot wire resistance (R_0). With the help of known temperature coefficient of resistivity (α_0) and Over Heat Ratio (OHR), we can calculate the hot wire temperature (T_{wire}) using the Equation (2.10). Once we get the hot wire temperature, we can calculate the film properties such as film temperature (T_{film}), dynamic viscosity (μ) and density of the film (ρ) using Equation (2.11) and Equation (2.12).

The velocity (u) of the flow is calculated using Equation (2.16).

$$u = \left(\left(\left(\frac{E^2}{OHR \times R_0} \right) \times \frac{1}{(T_{wire} - T_{gas})} \times \left(\frac{T_{gas}}{T_{wire} + T_{gas}} \right)^{0.17} \times \frac{1}{B} \right)^{\frac{1}{n}} \right) \times \left(\frac{\mu}{\rho} \right) \quad (2.16)$$

Once the velocity (u) is calculated, we will again calculate the Mach number (M_2) using Equation (2.17).

$$M_2 = \frac{u}{\sqrt{\gamma R T_{film}}} \quad (2.17)$$

Now we are defining an Error as shown in Equation (2.7). We are going to iterate the above process until we get an error less than 10^{-4} . In this way we will be calculating the velocity of the flow. Yasa et al. [1] also gives a method to calculate the turbulence intensity $Tu(\%)$ using the voltage output of the hot wire (E) and calibration constant 'n', it is shown in Equation (2.18), where \bar{E} is mean voltage and E' is voltage fluctuation around its mean value.

$$Tu(\%) = 100 \times \frac{2 \times \sqrt{\overline{E'^2}}}{n \times \bar{E}} \quad (2.18)$$

Flows in the test section are generally turbulent and they are comprising of eddies of different sizes [4]. There are two main quantities with which we define turbulent property of the flow: integral

length scale and dissipative length scale. Integral length scale tells us about the size of the large energy containing eddies while dissipative length scale tells us about the size of the dissipating eddies [4]. With the use of the hot wire we can obtain the information regarding the length scales of the turbulent flow. In the paper of P. E. Roach [19], he gave us a way to calculate the length scales using hot wire which was verified and used by Lamyaa A. El-Gabry. et al.[2]. Following equations tells us about the way to calculate the length scales from the hot wire, where λ_x is dissipative length scale and I_x is integral length scale, f is frequency, U is velocity of the flow, U_{mean} is mean of the velocity, u is velocity fluctuation around its mean value, \bar{u} is mean of u .

$$\frac{1}{\lambda_x^2} = \frac{2\pi^2}{U^2 \bar{u}^2} \int_0^\infty f^2 E(f) df \quad (2.19)$$

$$I_x = \left[\frac{E(f) U_{mean}}{4 \bar{u}^2} \right]_{f \rightarrow 0} \quad (2.20)$$

3. MODERN MANUFACTURING TECHNIQUES FOR THE DEVELOPMENT OF THE LAB

The goal that I share with my research team is to create an efficient system with which we can experiment on different articles and structures within few days of designing. In research, there is often a need for custom instrumentation and parts. Such components are generally contracted out to companies for manufacture. This process consumes significant amount of time and research funding. Because of the limited amount of resources available to researchers, this might potentially hamper the efficiency of the research work.

To mitigate these problems, we decided to pursue inhouse manufacturing. Inhouse manufacturing provides us with the benefit of low cost of operation and less time in manufacturing. Purdue university provides us with various facilities and equipment for the various manufacturing processes. Exploring these manufacturing techniques allowed me to prepare many experimental equipment that I used during my experimental campaign. In this chapter, we will be discussing about the manufacturing facilities utilized for the development of the lab.

3.1 Abrasive Cutting Operation

Abrasive cutting is a techniques where abrasive machining processes are used to cut the materials. Some of the tradition tools include waterjet, abrasive saw, grinder, etc. In this section we will be discussing about the waterjet abrasive cutting technique. Waterjet is a manufacturing machine which uses high pressured water to cut the materials [13]. In the past waterjet was only used to cut soft materials like rubber and paper with the help of high-pressured water going to through small diameter nozzle. As the research on waterjet evolved, waterjet cutting with the abrasive particles was introduced in 1935 [12]. This new technique helped in equipping the waterjet with the ability to cut very hard materials. Working of the waterjet abrasive cutting is shown in the Figure 3.1.

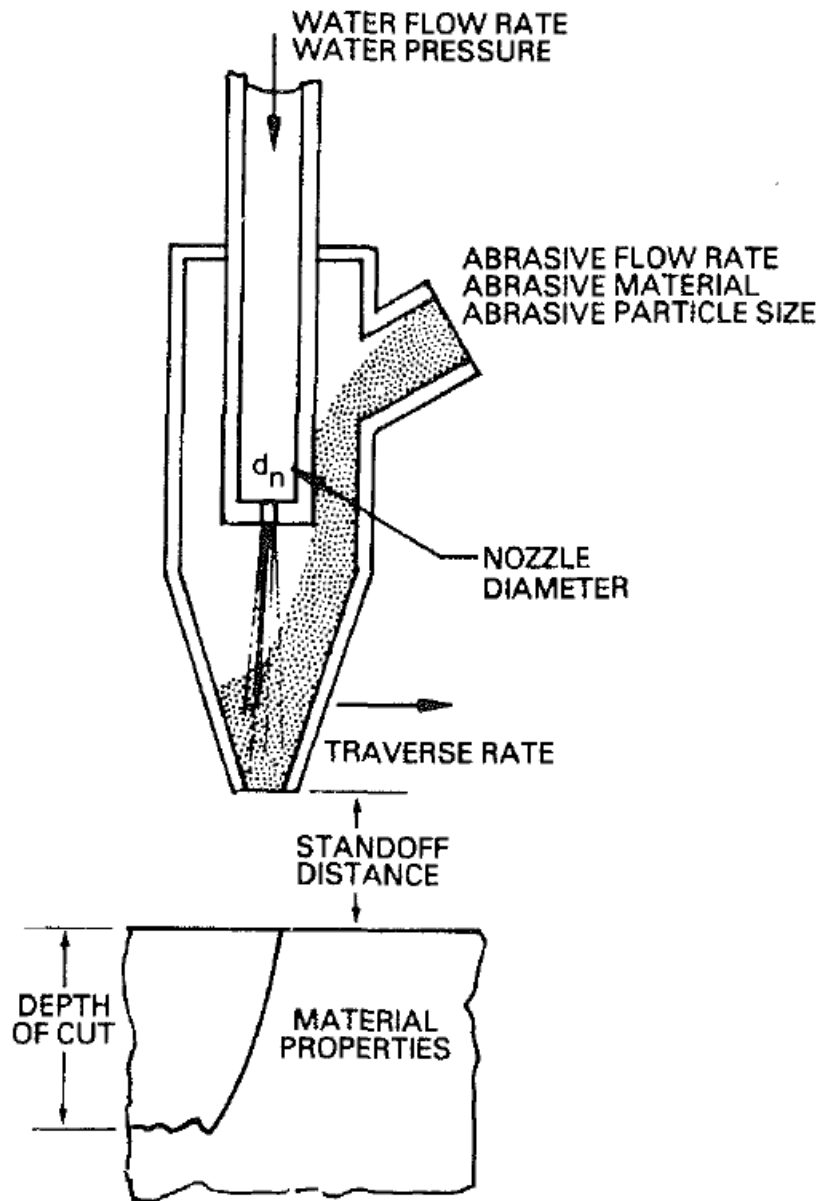


Figure 3.1 Waterjet nozzle operation [11].

As shown in Figure 3.1, high pressured water flows through high pressure tubes and it passes through the nozzle where it mixes with the abrasive material (generally known as garnet) flow. This mixture of abrasive and water is used to cut the hard materials.

The waterjet machine that was used in various machining operations for manufacturing the lab equipment is located at Bechtel Innovation Design Center (BIDC) as shown in Figure 3.2.

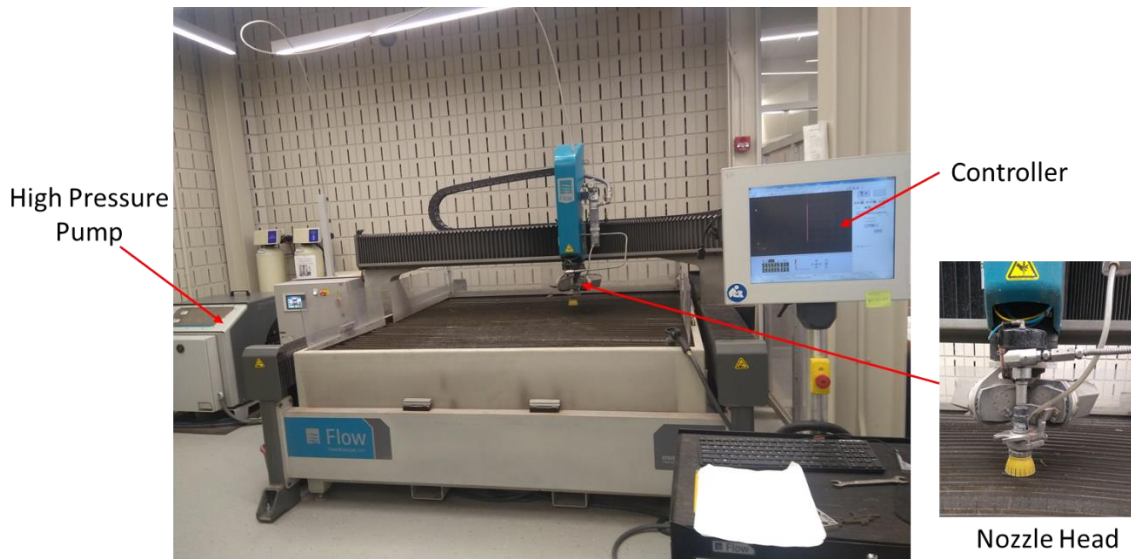


Figure 3.2 Waterjet machine at BIDC.

Waterjet machine as shown in Figure 3.2, is used to make 2D profiled equipment. Advantages of this machine over others are

- i. High operational speed
- ii. Ability to cut very large pieces of material
- iii. Ability to cut very hard materials (Tested with 6-inch-thick piece of Titanium)

In normal operational mode this machine has tolerance of ± 0.01 inch. Therefore, any part with tolerance limit more than mentioned is required, waterjet machine is preferred. In the case of roughing operations where accuracy or the surface finish of the parts is not the priority waterjet is highly sought-after machining process. If an accuracy up to ± 0.001 inch is required, then machine does have the capability to deliver that accuracy, but it takes longer time to calibrate the machine for the needed accuracy. Only in the case of part is very thin or part is very thick, or part size is large, waterjet operations are recommended.

3.2 Cold Machining Operations

Cold machining operations are the operations where the cutting tool does not heat up. In the development of the lab we have used two cold machining operations:

- i. Milling
- ii. Turning

3.2.1 Milling

Milling is a machining operation where a rotating cutter is used to remove the material from the work piece [14]. Milling machines dates backs to 1818 and since then the milling machines have evolved to modern Computer Numerical Control (CNC) milling machines [14]. First CNC milling machine was invented by William M. Pease and James O. McDonough in 1950, this CNC machine was controlled by the data on the Punched paper tape [15]. The current CNC machines are controlled through the computers. With the use of Computer Aided Machining (CAM), we are now capable of manufacturing complex geometries with the help of CNC milling machines. CNC milling machine used for manufacturing the lab equipment is located at Bechtel Innovation Design Center (BIDC) as shown in Figure 3.3 and Figure 3.4.

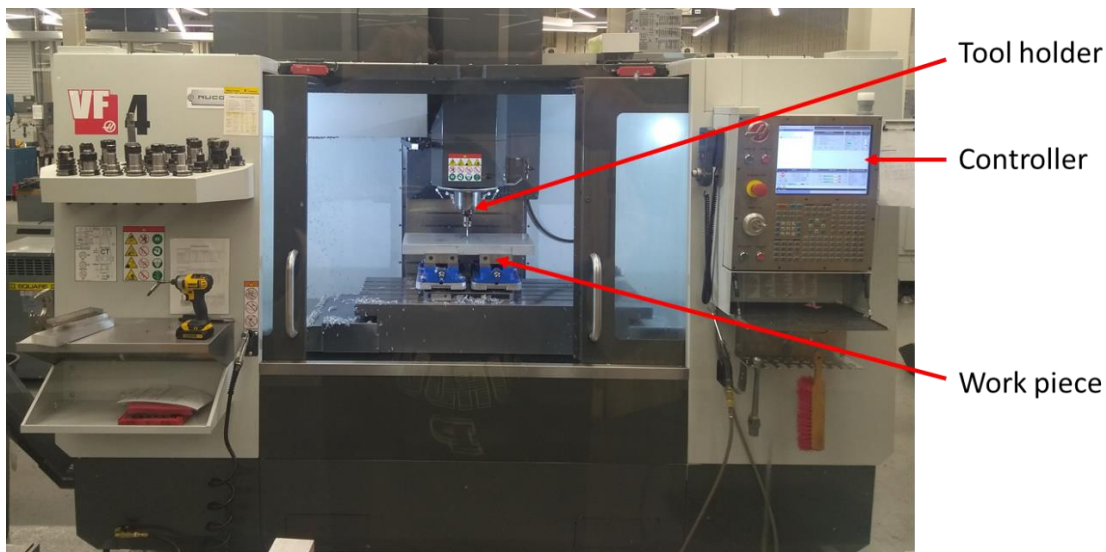


Figure 3.3 3-Axis CNC milling machine.

BIDC has two different types of CNC milling machines:

- i. 3-Axis CNC milling machine (Figure 3.3)
- ii. 5-Axis CNC milling machine (Figure 3.4)

This provides the users with the capability to machine complex geometries. The advantages these machines provide are:

- i. Complex 3D profiling
- ii. Fast operational speed
- iii. High accuracy, precision, reliability
- iv. Low tolerances

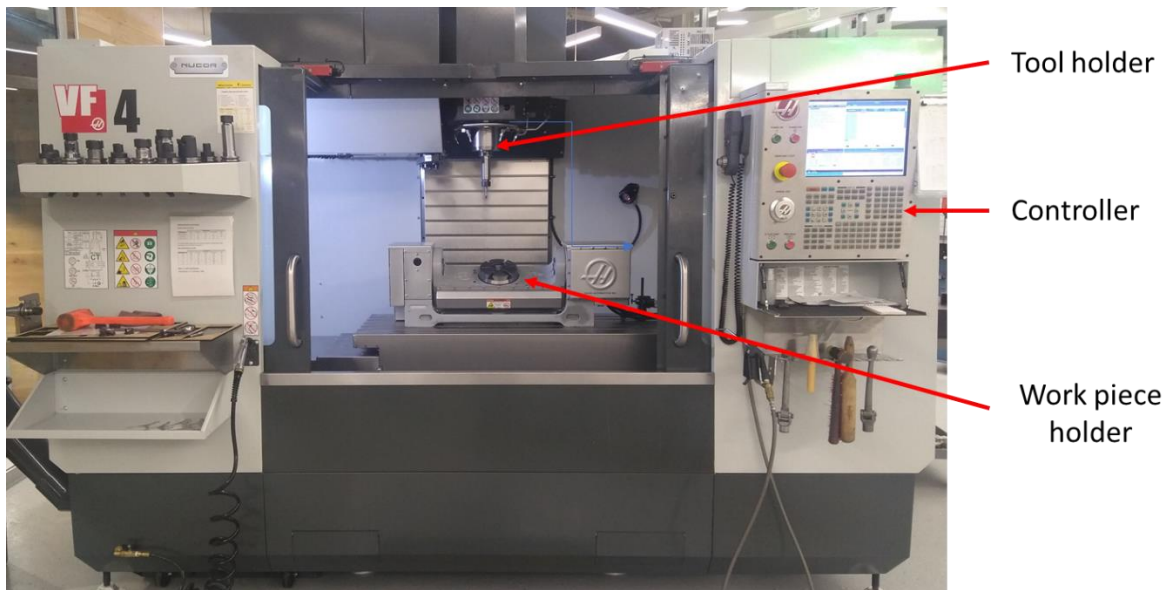


Figure 3.4 5-Axis CNC milling machine.

The basic operations that are done on these CNC milling machines are [22]:

- i. Drilling
- ii. Face milling
- iii. Straight milling
- iv. Thread milling
- v. Pocket milling
- vi. Contour milling
- vii. O-ring Groove milling
- viii. Engraving

These various operations provided the flexibility needed for manufacturing various parts for the development of the lab. The accuracy of probing the work piece and tools gave the precision need for the equipment. Easy modification to the vices provided the flexibility to clamp complex parts.

3.2.2 Turning

Turning is a machining operation where a work piece rotates, and a cutter is used to remove the material [17]. Turning machines, we are going to discuss are a lathe machine. Early evidence of lathe machines dates to 3rd century BC. Since then it evolved to current high-performance CNC lathe machines. CNC lathe is able work on complex geometries where axial symmetry is present.

CNC lathe machine used for manufacturing the lab equipment is located at Bechtel Innovation Design Center (BIDC) as shown in Figure 3.5.

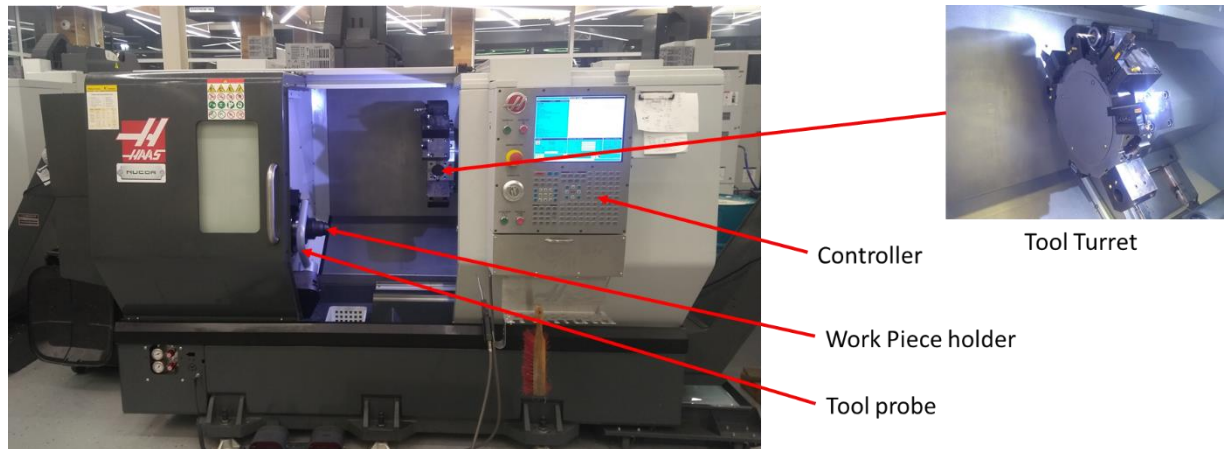


Figure 3.5 CNC lathe machine.

As shown in the Figure 3.5 a CNC lathe consists of a controller, tool turret, work piece holder, toll probe. This machine allows users to attain an accuracy of 0.001 inch during normal operations while more accurate operations are possible but requires time for calibration. The advantages of using the CNC lathe machines are:

- i. Complex axial profiling
- ii. Fast operational speed
- iii. High accuracy, precision, reliability
- iv. Low tolerances
- v. Live tooling

Live tooling is one of the amazing features that is also available for users which allows for machining capability besides axial geometries. In crude way it is a CNC mill in lathe this allowed us making complex parts in the lathe. The basic operations that are done on these CNC milling machines are [23]:

- i. Turning and facing
- ii. 2D contours
- iii. Drilling and taping
- iv. Threading
- v. Grooving

These various operations provided the flexibility needed for manufacturing various parts for the development of the lab. The accuracy of probing the work piece and tools gave the precision need for the equipment.

3.3 Manufactured Equipment

With the help of modern manufacturing machines mentioned in the previous sections as well as traditional manufacturing machines like drill press, belt sanders, band saw, power tools many of the lab equipment were built and are still being built. Some of the examples of such built parts will be shown in the following figures.

In the Figure 3.6, we can see the instrumentation equipment and their complete assembly. Figure 3.6 a) and Figure 3.6 b) are the instrumentation inserts made to hold various sensors for the experiments. To manufacture these inserts, we used waterjet to cut out the rough work piece from the available stock. Afterwards it was processed in the CNC mill to complete the manufacturing with the good surface finish. In the Figure 3.6 c) we can see the instrumentation support. The part is processed in the CNC mill to have great surface finish and due to its 3D geometry. Figure 3.6 d) shows the complete assembly of the instrumentation equipment used during the experiments.

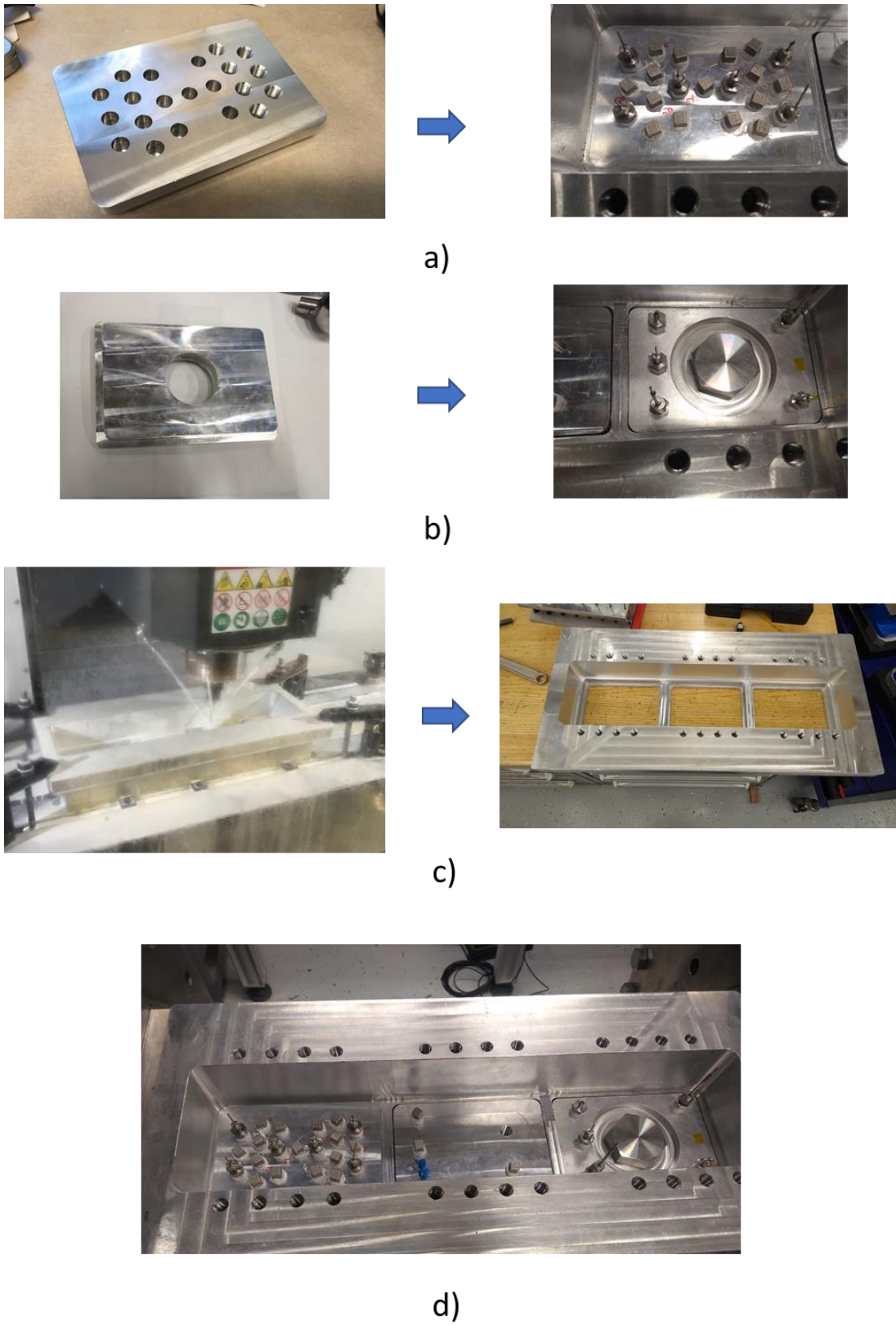


Figure 3.6 Instrumentation equipment: a) insert1 b) insert2 c) support and d) assembly.

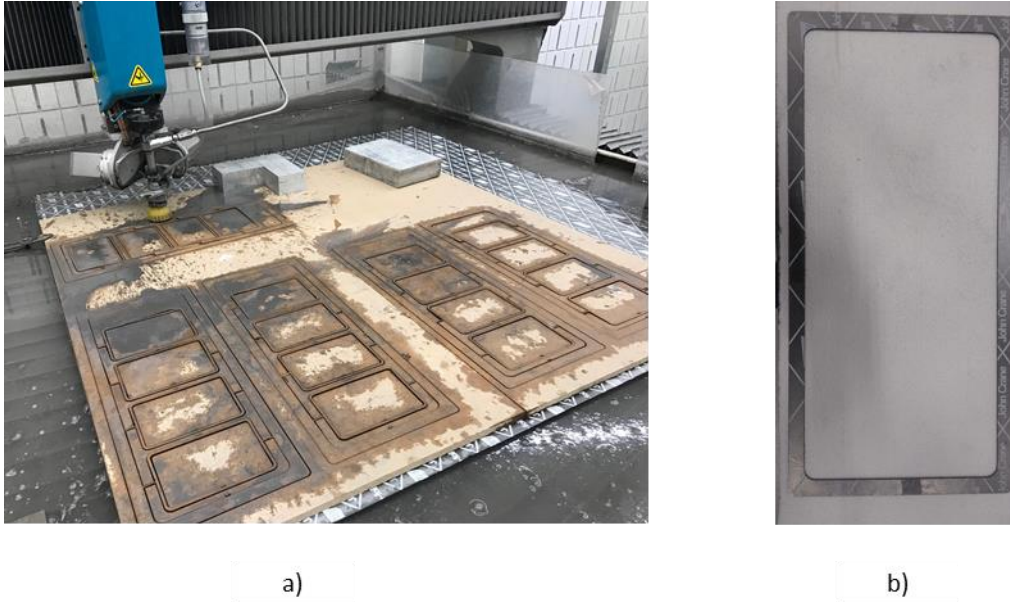


Figure 3.7 Graphoil gasket a) manufacturing of the gasket and b) manufactured gasket.

Graphoil gaskets are used to seal the instrumentation inserts, blank inserts and windows to prevent leakages in the linear wind tunnel. Graphoil is very soft material and can easily break. Because of it, they are only machined in the waterjet. To make sure graphoil sheet remains intact after machining, they are sandwiched between the wooden boards. It allows extra support to the material and prevents any accidental damage to the gaskets during the handling of the material. Machining process of the gaskets in the waterjet is shown in the Figure 3.7 a) with the finished blank insert gasket shown in Figure 3.7 b).

4. EXPERIMENTAL RESULTS

Experiments were conducted in the linear wind tunnel at the Purdue experimental turbine aerothermal lab. Results of six conditions are presented. The facilities were only available for six days. Each experiment took one day to achieve a single stable data condition.

For this experiment we used three static pressure sensors, six total pressure sensors and two total temperature sensors. The sampling rate of each sensor is as follows

- i. Pressure sensors (pressure tubes): 500 Hz
- ii. Temperature sensors (thermocouples): 1000 Hz
- iii. Hot wire sensor: 128 kHz

We are using thermocouple to measure total temperature. The fastest response 150 Hz of the thermocouples corresponds to a low-pass cut-off frequency. The data acquisition system allows us to sample thermocouple at maximum frequencies of 1000 Hz, which is 6 times higher than the cut-off frequency of the thermocouple. Using this sampling rate, we prevent aliasing in the temperature signal.

Pressure tubes are used to measure the total and static pressure. The tube length of the sensor is 3m long and diameter 0.0625 inch, which means that the maximum frequency we can resolve is less than 1 Hz. We use the maximum sampling frequency, 500 Hz of the pressure sensing device which is much larger than the frequency we obtain from the sensor.

The CTA has an in-built anti-aliasing filter with a cut-off frequency of 60kHz and a roll-off rate of 40 dB/decade. The flow characteristics of interest are below 50 kHz. The sample rate was chosen to be 128 kHz, the maximum possible, which should result in little aliasing in the frequency region of interest (0-50kHz) due to the roll-off rate of the filter.

4.1 Selection of Time Window:

The selection of the stable time window is done by plotting the variable against a time. Then the timeframe is selected in a way where we will not get change in mean value of the variable above certain limit. We select such time windows for multiple variables and use the intersection of these windows as our final window. Process of selection of such window is shown below in Figure.4.1

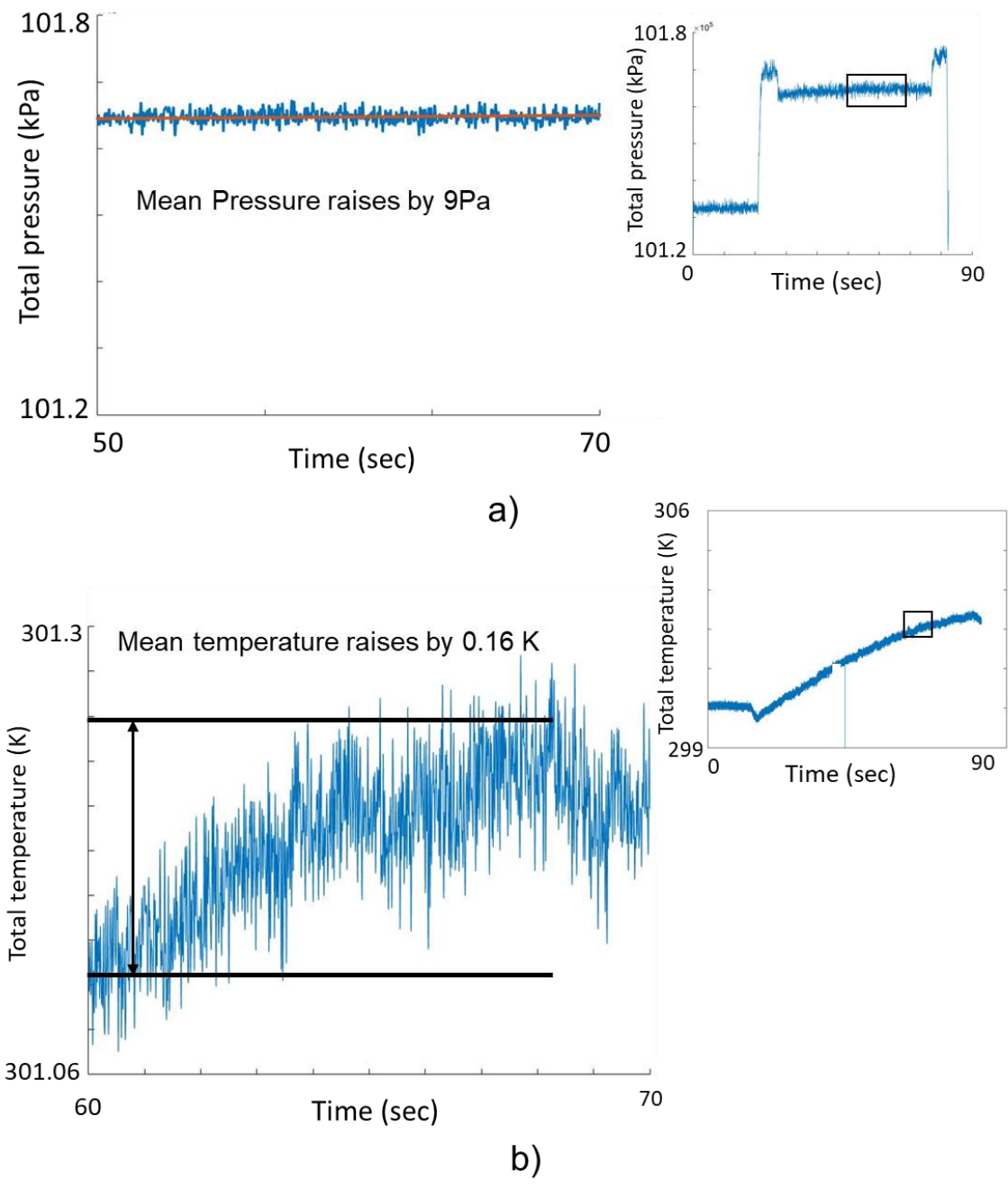


Figure 4.1 Time window selection for a) total pressure and b) total temperature.

For above case I found the time window from 50 to 70 seconds earns mean pressure change of 9 Pa. For pressure probes we kept that limit to 10 Pa. Therefore, this was accepted for reading. Similarly, for total temperature probe I found the time window from 60 to 70 seconds. For this period, the mean changed by 0.16 K. Therefore, it was accepted for reading. The common window

is 60 to 70 seconds. Similarly, the readings were taken for other sensors and in similar manner we have selected the windows. For thermocouple we kept the limit at 0.2 K and for hot wire at 0.1V.

4.2 Hot Wire Calibration Results

4.2.1 Pressure Data

Once we gather the raw data from the pressure sensors, we choose the most stable region to measure the pressure values from each sensor. In case if a sensor is damaged or shows erratic behavior, we do not consider the data from that sensor for the calibration. In Figure 4.2 we can see the plot of the static pressure data from one of the static pressure sensors at three different conditions. In Figure 4.3 we can see the plot of the total pressure data from one of the total pressure sensors with the same conditions. Table 4.1 gives us a summary of the pressure data used for the Hot Wire calibration for different conditions.

Table 4.1 Calibration data of the pressure sensors with standard deviation of the estimated mean in magnitude of 10^{-1} Pa.

Condition	Static Pressure (KPa)	Total Pressure (KPa)
1	101.37	101.45
2	101.38	101.47
3	101.42	101.63
4	101.43	101.68
5	101.49	101.87
6	101.57	102.15

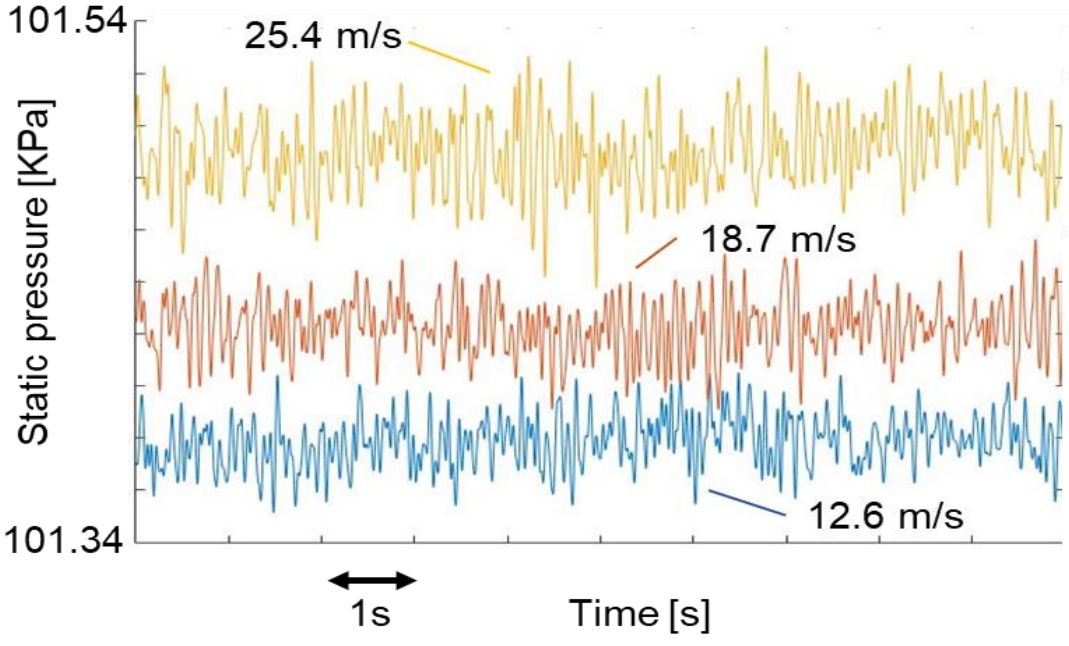


Figure 4.2 Static pressure in a stable region for three different velocities.

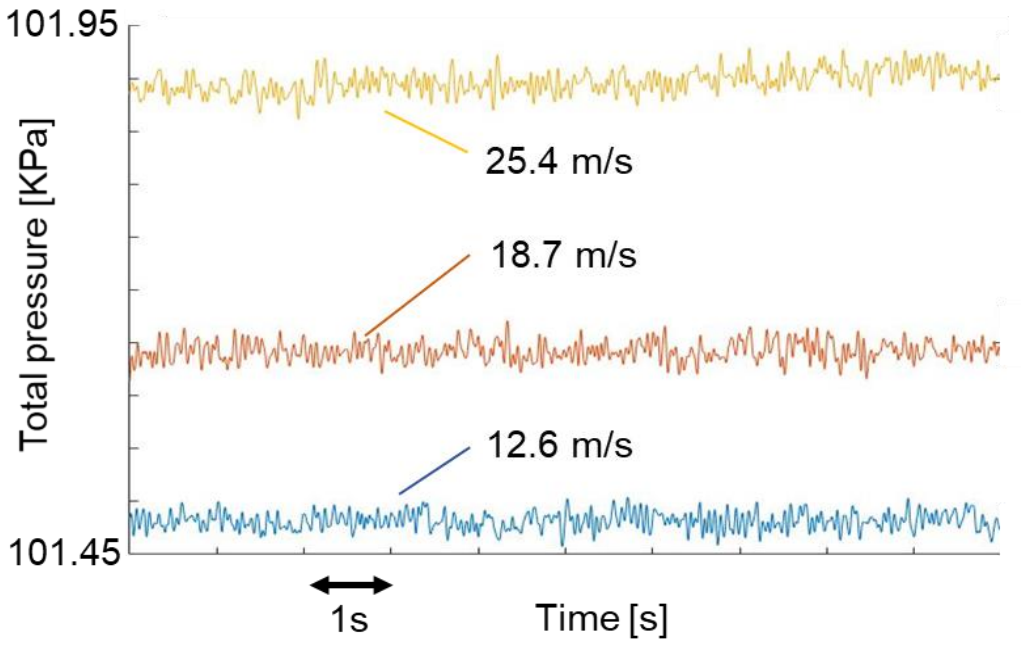


Figure 4.3 Total pressure in a stable region for three different velocities.

4.2.2 Temperature Data

Once we gather the raw data from the temperature sensors, we choose the most stable region to measure the temperature values from both sensors. The thermocouple sensors used in this experiment is used to get the total temperature. In Figure 4.4 we can see the plot of the total temperature data from one of the total temperature sensors with the same conditions as used in the pressure data plot. We use this data to calculate the static temperature for each condition using the method discussed in section 2.2.1. Table 4.2 gives us a summary of the temperature data used for the Hot Wire calibration for different conditions.

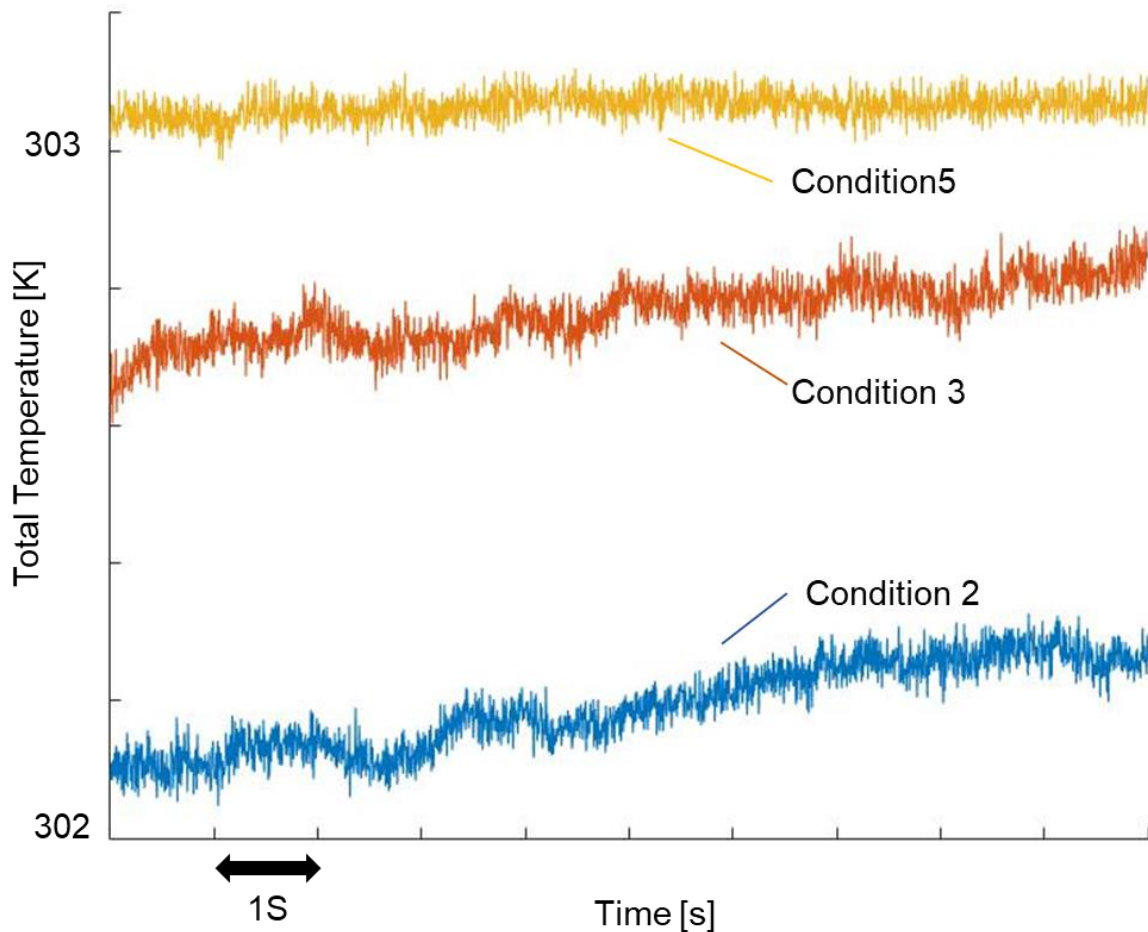


Figure 4.4 Total temperature data in a stable region for three different velocities.

Table 4.2 Calibration data of the Temperature with standard deviation of the estimated mean in magnitude of 10^{-3} K.

Condition	Static Temperature (K)	Total Temperature (K)
1	302.25	302.32
2	301.62	301.71
3	302.57	302.76
4	302.67	302.88
5	302.61	302.93
6	302.10	302.59

4.2.3 Hot Wire Voltage Data

Once we gather the raw data from the CTA module, we choose the most stable region to measure the voltage values on the hot wire sensors. In Figure 4.5 we can see the plot of the voltage data from the hot wire sensors with the same conditions as used in the pressure data plot. Table 4.3 gives us a summary of the voltage data used for the Hot Wire calibration for different conditions.

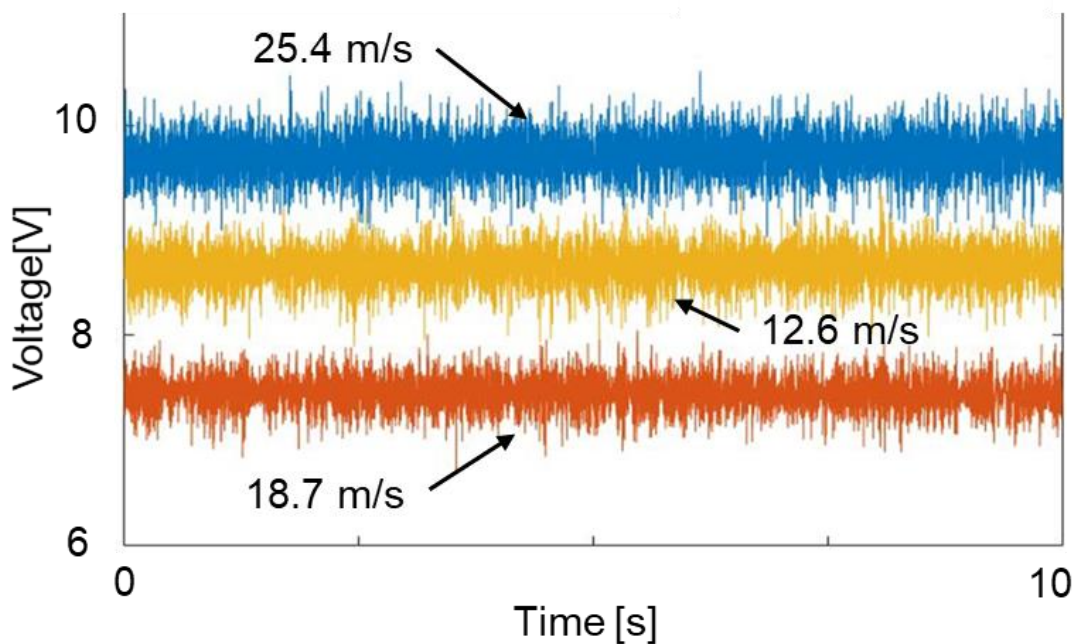


Figure 4.5 Voltage of hot wire in a stable region for three different velocities.

Table 4.3 Calibration data of the Hot Wire sensor with standard deviation of the estimated mean in magnitude of 10^{-4} V.

Condition	Hot Wire reading (V)
1	7.21
2	7.45
3	8.66
4	8.93
5	9.71
6	10.50

4.2.4 Hot Wire Calibration Result

The collected data is then used to calibrate the hot wire using the method discussed in section 2.2.1. Velocity measured for each condition is tabulated in Table 4.4.

Table 4.4 Calibration data of velocity.

Condition	Velocity (m/s)
1	11.8
2	12.6
3	18.7
4	20.3
5	25.4
6	31.4

From the calibration we got following information

- i. $B = 4.56 \times 10^{-7}$
- ii. $n = 0.763$
- iii. $R^2_{adjusted} = 0.9995$

$R^2_{adjusted}$ value was calculated using following Equation (4.2) where Y_i is i^{th} measured values, \bar{Y} is mean of Y and Z_i is the i^{th} predicted value of Y :

$$R^2_{adjusted} = 1 - \frac{(np - 1) \sum_{i=1}^{np} (Z_i - Y_i)^2}{(np - p) \sum_{i=1}^{np} (Y_i - \bar{Y})^2} \quad (4.1)$$

Where np is number of data points and p is number of variables. For our case np is 6 and p is 2. The results of the optimization are shown in the Figure 4.6.

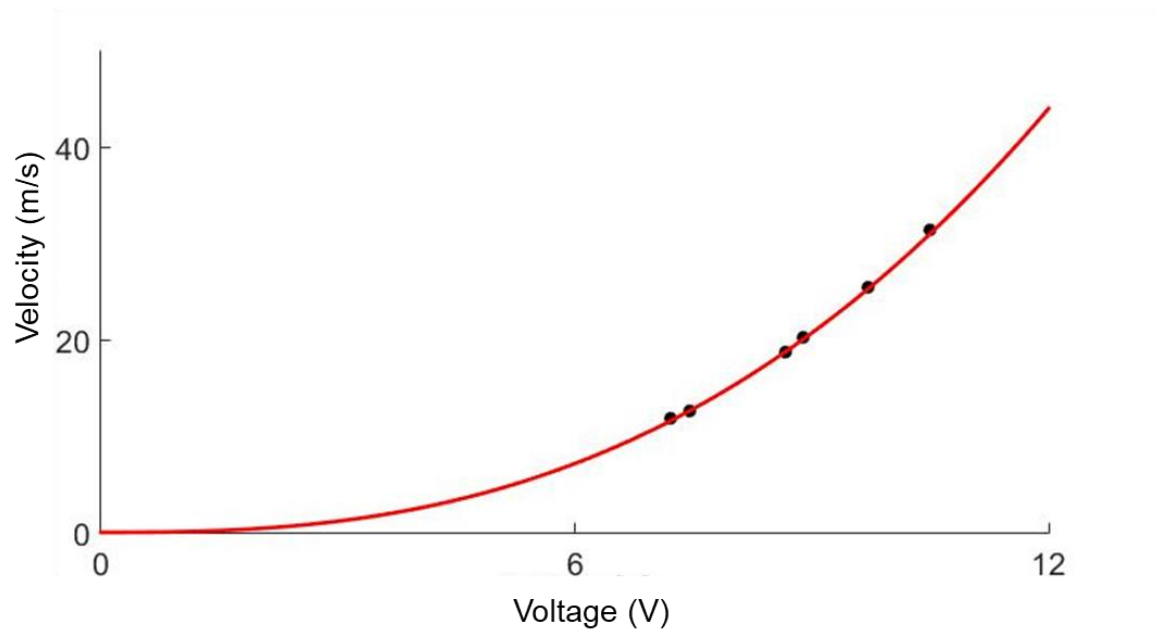


Figure 4.6 Curve fitting plot.

4.3 Hot Wire Post Process Results

We use the hot wire calibration to characterize the flow inside the wind tunnel. Using the methods shown in the section 2.2.2 we are going to calculate turbulence intensity, integral length scale, dissipative length scale and the velocity for the experiment. Velocity plot for three different experimental conditions is shown in Figure 4.7.

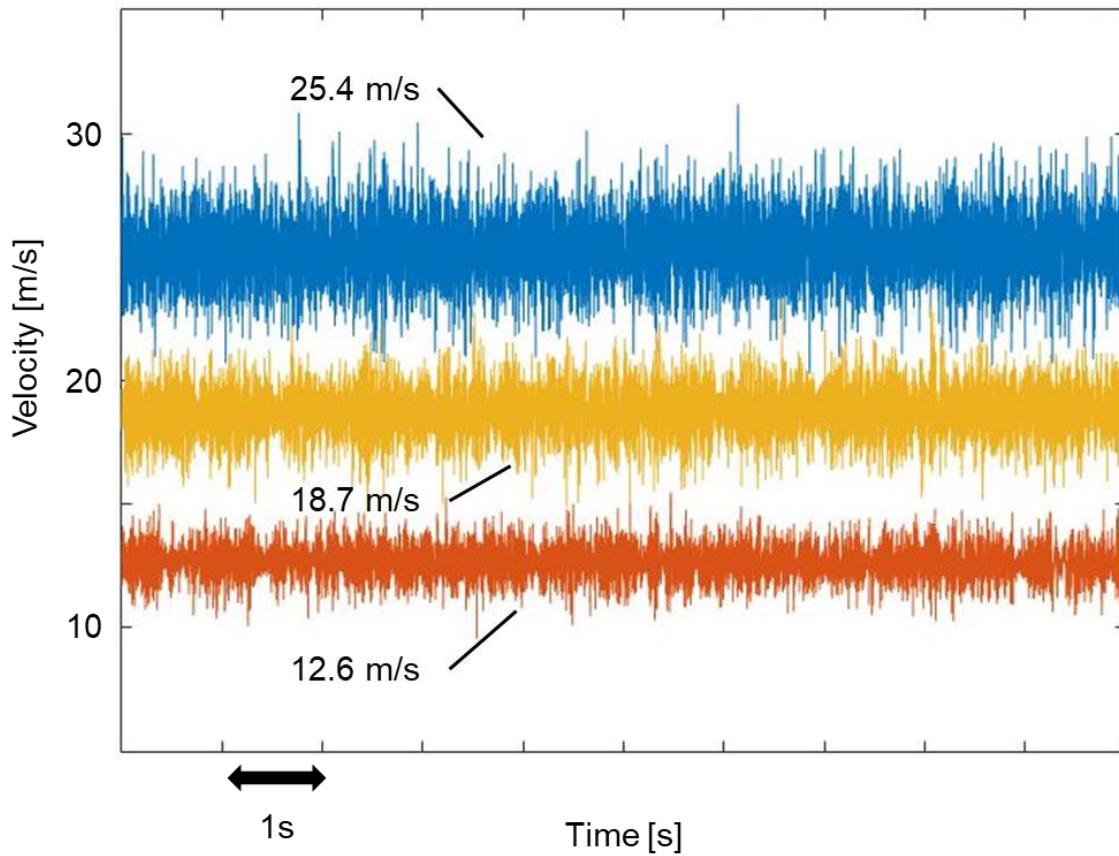


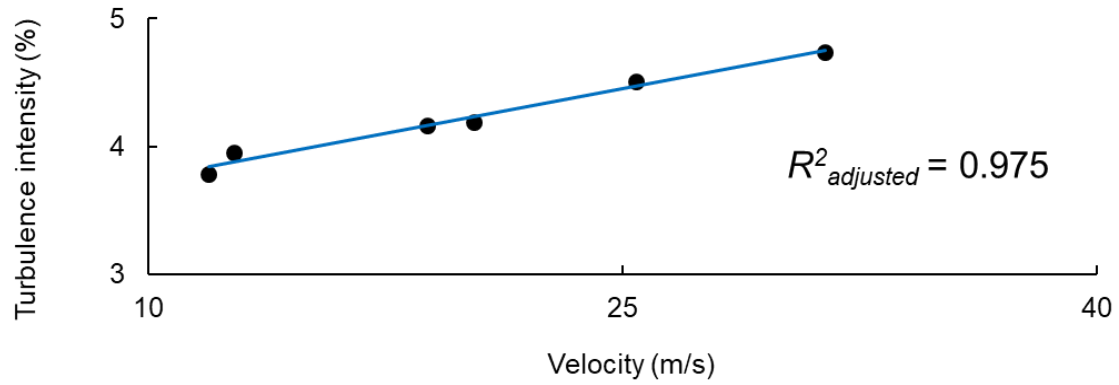
Figure 4.7 Velocity plot in a stable region for three different velocities.

Turbulence property measurements are tabulated in the Table 4.5.

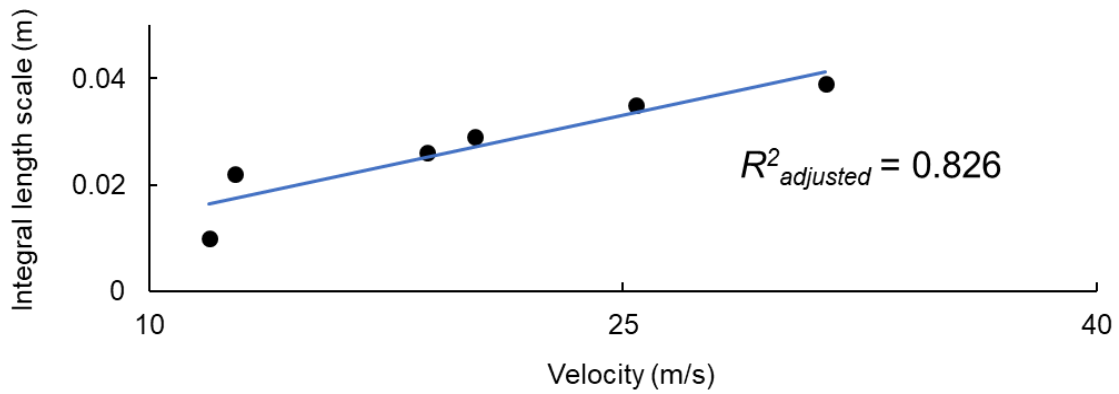
Table 4.5 Turbulent property.

Condition	Turbulence intensity (Tu %)	Integral length scale (m)	Dissipative length scale (mm)
1	3.78	0.010	1.1
2	3.95	0.022	1.2
3	4.16	0.026	1.5
4	4.19	0.029	1.6
5	4.51	0.035	1.8
6	4.74	0.039	2.2

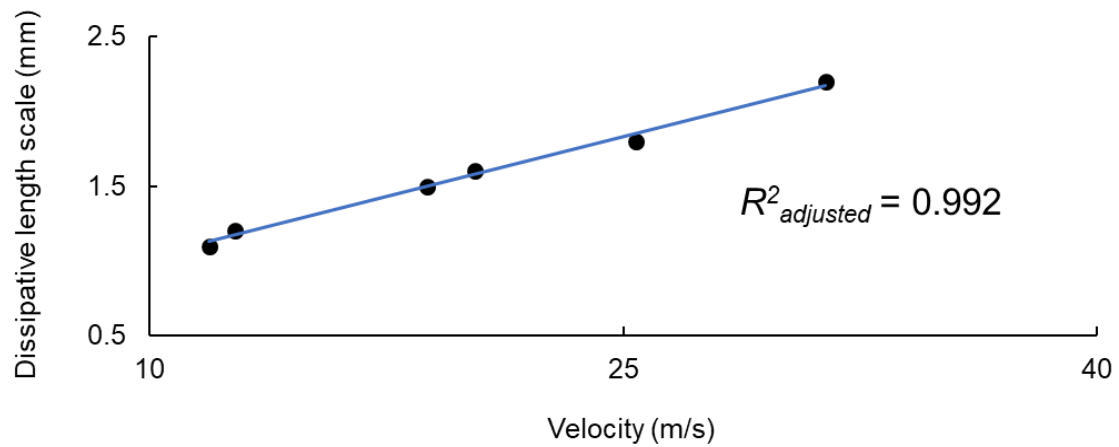
To see the trend of the different turbulence properties with change in the velocity is then plotted and is shown in Figure 4.8. From the Figure 4.8 a) we can see that turbulence intensity (%) shows a linear behavior with the change in the velocity with $R^2_{adjusted}$ value of 0.975. This way we might be able to predict the turbulence intensity within the region for different velocities.



a)



b)



c)

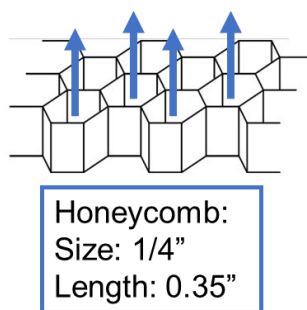
Figure 4.8 Turbulence properties plotted against velocity a) turbulence intensity (%) b) integral length scale and c) dissipative length scale.

From the Figure 4.8 b) we see that except for the first two data point the integral length scale shows a quasi-linear behavior with respect to the change in velocity. It also observed that integral length is in ratio with multiplication of honeycomb cell size and velocity with $R^2_{adjusted}$ value of 0.826. This might help in predicting the behavior of the integral length scale in the region of the quasi linear behavior. From the Figure 4.8 c) we can see that the dissipative length scale shows a linear behavior with the change in the velocity with $R^2_{adjusted}$ value of 0.992. This way we might be able to predict the dissipative length scale within the region for different velocities.

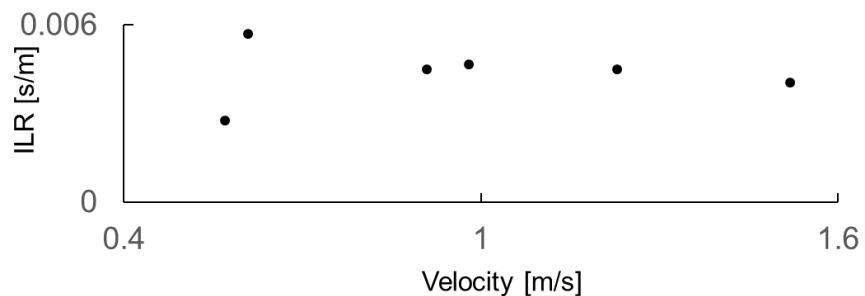
We further tried to investigate integral length scale and honeycomb structure inside of the settling chamber. We defined a variable ILR which is a ration of integral length scale to the velocity inside the settling chamber and the size of the honeycomb. It is tabulated and plotted in the Table 4.6 and Figure 4.9. We can see that at relatively higher velocities we get a constant ratio. This might help us in predicting the ration at higher velocity range.

Table 4.6 Integral length scale ratio data.

Condition	Settling Chamber Velocity (m/s)	<i>Integral Length Scale</i>
		$\frac{\text{Velocity} \times \text{Size of Honeycomb}}{\text{ILR(s/m)}}$
1	0.57	0.0027
2	0.61	0.0056
3	0.91	0.0044
4	0.98	0.0046
5	1.23	0.0044
6	1.52	0.0040



a)



b)

Figure 4.9 a) Honeycomb structure and b) ILR vs velocity plot.

4.4 Uncertainty Analysis

To calculate the uncertainty of a calculated variable C which is dependent on ‘N’ independent variables (X_1 to X_n), we can define uncertainty using the method described by Kline and McClintock [25]. X_i is an i^{th} independent variable. Here, δ_{x_i} is an individual uncertainty in the variable X_i . The effect of uncertainty in variable x_i considering only that variable has an error in measurement then it can be computed using Equation 4.4.

$$C = f(X_1, \dots, X_i, \dots, X_n) \quad (4.3)$$

$$\delta C_{X_i} = \frac{\partial C}{\partial X_i} \delta X_i \quad (4.4)$$

Here sensitivity coefficient of C with respect to the independent variable X_i is given by the partial derivative of the of result C with respect to the independent variable X_i . The total contribution of all the independent variables on the total uncertainty is given by Equation 4.5.

$$\delta C = \left\{ \sum_{i=1}^N \left(\frac{\partial C}{\partial X_i} \delta X_i \right)^2 \right\}^{\frac{1}{2}} \quad (4.5)$$

When A is computed using a computer program the uncertainty and sensitivity of the process is calculated using the method of R. J. Moffat [21]. For these calculations, the data interpretation program is used to generate the uncertainty analysis, by sequentially perturbing the input values and accumulating the individual uncertainty contributions [21]. Steps for the computation are as follows:

- i. For experimentation we store the value of the mean of variable C : C_0
- ii. For all the variables X_i we are going to do following procedure: First we add the uncertainty δ_{x_i} in the variable X_i and then calculate the C_{ui} , which is values of variable C due to uncertainty in the variable X_i , by keeping other variables at their mean values. Now we calculate the change in C due to the uncertainty in X_i as $\Delta C_{ui} = |C - C_{ui}|$. We repeat this procedure to get the individual uncertainty of all the variables.
- iii. To calculate the total uncertainty of the process we take the square root of the sum of squares of individual contribution as shown in Equation 4.6.

$$(\Delta C_u)^2 = \sum_{i=1}^n (\Delta C_{u_i})^2 \quad (4.6)$$

Sensitivity of the variables tells us how much a dependent variable change by changing the variable by a unit value. To calculate the sensitivity of the variables we use Equation 4.7.

$$Sensitivity(\%) = \frac{\Delta A_{u_i}}{\frac{\delta_{X_i}}{X_i}} \times 100 \quad (4.7)$$

For uncertainty and sensitivity analysis, the absolute uncertainty of each variable is based on repeated experiment and statistical analysis. For example, absolute uncertainty of T_0 : 1K was obtained in the previous experimental campaign.

Table 4.7 Uncertainty calculation for velocity.

	Mean	Unit	Uncertainty	v with Uncertainty	Δv (%)	Sensitivity (%)
P_0	101675.61	Pa	50	20.29	0	0
P	101434.8697	Pa	50	20.28	0.049	99.98
T_0	299.98	K	1	20.32	0.14	44.35
R_0	13.1	Ω	0.01	20.35	0.29	387.38
α	0.0009	1/K	0.00005	20.33	0.19	3.54
E	8.93	V	0.001	20.29	0.006	53.58
n	0.763		0.0002	20.28	0.049	188.02
B	4.56×10^{-7}		0.00000026	19.44	4.19	7.41
Velocity v	20.29	m/s		Total uncertainty	4.23	

Total uncertainty for velocity as shown in above Table 4.7 is a square root of sum of square of individual contribution of the uncertainty of independent variable. Hot wire measurement technique has uncertainty of 4.23%. The most sensitive variables for the calibration are R_0 and n . Uncertainty in turbulence intensity came out as 0.029% for condition 4. The calculations for it are shown in Table 4.8.

Table 4.8 Uncertainty calculation for Turbulence intensity.

	Mean	Unit	Absolute Uncertainty	Tu with uncertainty (10^{-2})	$\Delta Tu(\%)$
E	8.93	V	0.001	4.186	0.011
n	0.763		0.0002	4.185	0.026
Tu	4.187				0.029

Following properties only depend on velocity of the flow I have used the uncertainty calculated in Table 4.7 to find the uncertainties in these properties. Uncertainty in Integral length scale for condition came out to be 4.22% as shown in Table 4.9.

Table 4.9 Uncertainty calculation for Integral length scale.

	Mean	Unit	Absolute Uncertainty	ILS with uncertainty	$\Delta ILS(\%)$
Velocity	20.29	m/s	0.86	0.030	4.22
ILS	0.029	m			4.22

Uncertainty in dissipative length scale for condition came out to be 4.27% as shown in Table 4.10.

Table 4.10 Uncertainty calculation for Dissipative length scale.

	Mean	Unit	Absolute Uncertainty	DLS with uncertainty	$\Delta DLS(\%)$
Velocity	20.29	m/s	0.86	1.66	4.27
DLS	1.59	mm			4.27

5. CONCLUSIONS

Through this work we have characterized the Purdue Experimental Turbine Aerothermal Lab rig using hot wire anemometry measurement technique. Based on the recent literature, hot wire anemometry was used for this characterization taking into account the temperature correction of the data. A suitable data acquisition procedure is developed for the successful utilization of the sensor. Development of this data acquisition procedure was fundamentally based on using the existing in-house sensors. For the data acquisition procedure of the hot-wire sensor, total pressure sensors, static pressure sensors, total temperature sensors were used to develop the technique. **With the help of these sensors a data acquisition system was successfully developed.**

Hot wire calibration is done before every experiment. In the novel procedure, we used available sensors to compute the velocity of the flow and match it with the hot wire sensor using a calibration law. The calibration process was done in the linear wind tunnel. For the calibration process we have used the CTA module, total pressure sensors, static pressure sensors, total temperature sensors. During the calibration we choose stable data points on which our calibration was based on. During the calibration process minor adjustments are also made to make sure the hot wire response will be within the acceptable range of the data acquisition system. **The calibration technique was validated during the experimental campaign with a $R^2_{adjusted}$ value of 0.9995.**

Custom instrumentation and parts were needed for the development of the lab. For this, various modern manufacturing techniques were investigated to better understand the manufacturing process. It helped in designing the equipment based on the capability of the machines and making them manufacturable inhouse. **Understanding and utilizing the manufacturing techniques successfully helped in manufacturing experimental equipment for complex geometries.**

Successfully calibrated hot wire was used to characterize the Purdue Experimental Turbine Aerothermal Lab rig. For the successful utilization of hot wire probe, we have developed the hot wire post process method. **Post process method was successfully tested and utilized for the experiment. We computed the velocities, turbulence intensity, turbulence length scales and uncertainty associated to the measurements at different velocities of the flow.**

With this work, we have successfully developed the hot wire measurement technique for the characterization of the Purdue Experimental Turbine Aerothermal Lab rig

APPENDIX

3D Printing

3D printers are part of additive manufacturing where equipment are made layer by layer process. 3D printing technique made the evolutionary change in manufacturing industry. It allowed a very complex design to be manufactured with high precision. The 3D printing facility used in the development of the lab are in B IDC and BoilerMAKER lab.

3D printers available to us comes up with different variety of materials. This allows to have flexibility in choosing the right material to meet the right requirements of the equipment function.

Benefits of this techniques are listed below:

- i. Very complex 3D design manufacturing
- ii. Fast operational speed
- iii. High accuracy, precision
- iv. Low tolerances
- v. Low cost

3D printing allows to manufacture equipment that are impossible to manufacture using any other techniques mentioned before. It allows us to prepare test articles for low temperature testing. It saved lot of time for preparing the needed equipment for testing. 3D printing allowed to verify the conceptual design that helped us in finalizing the designs. This technique was used to manufacture many needed hardware for the lab.

REFERENCES

- [1] Yasa, T., Paniagua, G., Denos, R, 2006, Application of Hot-Wire Anemometry in a Blow-Down Turbine Facility, ASME. J. Eng. Gas Turbines Power; 129(2):420-427. doi:10.1115/1.2364191.
- [2] El-Gabry, L., Thurman, D., Poinatte, P., Procedure for Determining Turbulence Length Scales Using Hotwire Anemometry, NASA/TM—2014-218403.
- [3] Stainback, P., Nagabushana, K., 1997, Review of Hot-Wire Anemometry Techniques and the Range of their Applicability for Various Flows, Electronic Journal of Fluids Engineering.
- [4] Bruun, H., 1995, Hot-Wire Anemometry Principles and Signal Analysis. Oxford Science Publication.
- [5] Fingerson, L., Thermal anemometry, current state, and future directions, Review of Scientific Instruments 65, 285 (1994).
- [6] King, L., 1914, On the Convection of Heat from Small Cylinders in a Stream of Fluid. Determination of Convective Constants of Small Platinum Wires with Application to Hot-wire Anemometry, Philos. Trans. R. Soc. London, Ser. A, 214, pp. 373–432.
- [7] Collis, D., and Williams, M., 1959, Two Dimensional Convection From Heated Wires at Low Reynolds Numbers, J. Fluid Mech., 16, pp. 357–384.
- [8] Analytical and Experimental Investigation About Heat Transfer of Hot-Wire Anemometry - Scientific Figure on ResearchGate, Available from: https://www.researchgate.net/Schematic-of-a-constant-temperature-anemometer_fig1_267037812 [accessed 26 Nov 2018].

- [9] Paniagua G., Cuadrado D., Saavedra J., et al., 2018, Design of the Purdue Experimental Turbine Aerothermal Laboratory for Optical and Surface Aerothermal Measurements. ASME. J. Eng. Gas Turbines Power.,141(1):012601-012601-13. doi:10.1115/1.4040683.
- [10] AN 1002-CTA Manual, A. A. Labs systems ltd.
- [11] Hashish M., 1984, A Modeling Study of Metal Cutting With Abrasive Waterjets, ASME. J. Eng. Mater. Technol., 106(1):88-100. doi:10.1115/1.3225682.
- [12] Smith, E., 1935, U.S. Patent No. US2040715A. Washington, DC: U.S. Patent and Trademark Office.
- [13] Momber, A., Kovacevic, R., 1998, Principles of Abrasive Water Jet Machining, Springer
- [14] Providence, R., 1919, Practical Treatise on Milling and Milling Machines, Brown & Sharpe Manufacturing Company.
- [15] MIT History Archives, Available from: <https://libraries.mit.edu/mithistory/research/labs/mit-servomechanisms-laboratory/> [accessed 21 Nov 2018].
- [16] Schurr, S., Burwell, C., Sonenblum, S., Devine, W., 1990, Electricity in the American Economy: Agent of Technological Progress, Greenwood Publishing Group
- [17] Encyclopedia Brintanica, Available form: <https://www.britannica.com/technology/lathe> [accessed 21 Nov 2018].
- [18] The Woodturner's Workshop, Available from: <http://www.turningtools.co.uk.wgo.ca/history2/history-turning2.html> [accessed 23 Nov 2018]
- [19] Roach, P., 1987, The generation of nearly isotropic turbulence by means of grids, International Journal of Heat and Fluid Flow, 8(2), pp.82-92.

- [21] Moffat, R., 1988, Describing the Uncertainties in Experimental Results, *Experimental Thermal and Fluid Science*, 0894-1777/8890043-X doi 1:3-17
- [22] HAAS Mill Manual
- [23] HAAS Lathe Manual
- [24] TSI Hot wire catalog
- [25] Kline, S. J., and McClintock, F. A., Describing Uncertainties in Single Sample Experiments, *Mech. Eng.*, 3-8, Jan. 1953.